ANL-6679

Argonne National Laboratory

PHYSICS DIVISION

SUMMARY REPORT

January-February 1963

ANL-6679
Physics
AEC Research and
Development Report

ARGONNE NATIONAL LABORATORY
9700 South Cass Avenue
Argonne, Illinois

PHYSICS DIVISION SUMMARY REPORT

January-February 1963

Lowell M. Bollinger, Division Director

Preceding Summary Reports

ANL-6603, July-August 1962
ANL-6612, September-October 1962
ANL-6666, November-December 1962

Operated by The University of Chicago

under

Contract W-31-109-eng-38

with the

U. S. Atomic Energy Commission

FOREWORD

The Summary Report of the Physics Division of the Argonne National Laboratory is issued monthly for the information of the members of the Division and a limited number of other persons interested in the progress of the work. Each active project reports about once in 3 months, on the average. Those not reported in a particular issue are listed separately in the Table of Contents with a reference to the last issue in which each appeared.

This is merely an informal progress report. The results and data therefore must be understood to be preliminary and tentative.

The issuance of these reports is not intended to constitute publication in any sense of the word. Final results either will be submitted for publication in regular professional journals or, in special cases, will be presented in ANL Topical Reports.

TABLE OF CONTENTS

The date of the last preceding report is indicated after the title of each project below. Active projects that are not reported in this issue are listed on subsequent pages.

PAGE

I. EXPERIMENTAL NUCLEAR PHYSICS

I-10-2 TANDEM VAN DE GRAAFF ACCELERATOR (ANL-6262, December 1960)

J. R. Wallace 1

A short chronological summary of the tandem Van de Graaff accelerator project and a summary of the tandem acceptance tests are given.

I-14-24 PULSED-BEAM EXPERIMENTS WITH THE VAN DE GRAAFF MACHINE (ANL-6391, July-August 1961)

F. J. Lynch and E. N. Shipley 5

We have studied the previously identified doublet near 245 keV in Se^{77} by use of Coulomb excitation and pulsed-beam techniques. The mean life of the weakly excited upper level at 249 keV was found to be 13.2 ± 1.2 nsec, so that it could be easily separated from the very short lived but strongly excited lower level. The relative intensities of the various de-excitation gamma rays were measured, and the $B(E2)_{exc}$ of the 249-keV level was found to be $(1.25 \pm 0.25) \times 10^{-50} e^2 cm^4$.

I-21-10 EXCITED STATES OF LIGHT NUCLEI (ANL-6603, July-August 1962)

J. A. Weinman 13

A procedure is described that enables either the particle width $\Gamma_{a\ell}$ or the total width Γ to be determined from elastic-scattering

PAGE

experiments when the target thickness T (in energy units) exceeds Γ.

I-27-1 STUDIES OF DEUTERON-INDUCED REACTIONS (New project)

J. P. Schiffer, L. L. Lee, Jr., and B. Zeidman 19

Absolute differential cross sections for the reactions Ca(d,d)Ca and $Ca^{40}(d,p)Ca^{41}$ have been measured. These results are a test for distorted-wave Born-approximation calculations of the stripping reaction.

I-31-3 ELASTIC SCATTERING OF PROTONS (ANL-6666, November-December 1962)

L. L. Lee, Jr. and J. P. Schiffer 23

Fluctuations in the excitation functions for scattering of protons from Ni have been studied with thin and thick targets. The results disagree with some of the expectations from the statistical model.

I-55-12 CAPTURE GAMMA-RAY SPECTRA FOR NEUTRONS WITH ENERGIES FROM 0.1 to 10 EV (ANL-6052, September 1959)

S. Raboy and C. C. Trail 26

The gamma-ray spectrum from neutron capture in Ca^{44} has been observed with a scintillation spectrometer having an anticoincidence annulus. Two spectrometers were used in coincidence to study the decay scheme. Some preliminary data are reported.

I-57-1 MU-MESONIC X RAYS FROM ATOMS WITH $7 \leqslant Z \leqslant 30$ (New project)

PAGE

C. S. Johnson, H. L. Anderson, E. P. Hincks, S. Raboy, and C. C. Trail 32

The scintillation spectrometer with an anti-coincidence annulus of NaI has been used to measure the energies of the 2p-1s transitions in mu-mesonic atoms with $7 \leq Z \leq 30$. About half of the data have been analyzed, and these results are reported.

II. MASS SPECTROSCOPY

II-26-1 IONIZATION BY IONS IN THE MEV RANGE (New project)

S. Wexler and D. C. Hess 47

The ionization of several of the rare gases and lower hydrocarbons by protons with energies from 0.80 to 3.75 MeV has been studied by mass-spectrometric methods. The portable mass spectrometer used for these investigations is described. Partial cross sections for production of rare gas ions in various charge states have been determined for this energy region.

II-40-11 FRAGMENTATION OF HYDROCARBONS (ANL-6534, April-May 1962)

H. E. Stanton and J. E. Monahan 56

A method is proposed for the analysis of measured energy distributions of ionic fragments resulting from electron impact on polyatomic molecules.

V. THEORETICAL PHYSICS, GENERAL

V-1-2 DEFORMATION ENERGY OF A CHARGED LIQUID DROP (ANL-6432, September-October 1961)

PAGE

63

S. Cohen and W. J. Swiatecki . . . . . .

The symmetric family of saddle-point shapes for charged liquid drops has been determined for values of the fissionability parameter x between 0.3 and 1.0. A transitional region in the neighborhood of x = 0.67 has been found. For x smaller than this value, the saddle-point shapes are dumbbell-like; for larger values they are cylinder-like. For x values larger than 0.39 the saddle point is found to correspond to a threshold for fission. For values smaller than 0.39 the saddle point is an unstable equilibrium point with respect to asymmetric distortions and therefore no true threshold exists.

V-11-1 RESONANCE THEORY OF NUCLEAR REACTIONS WITHOUT BOUNDARY CONDITIONS (New project)

69

A. M. Saperstein . . . . . .

Nuclear reactions are discussed by use of a dispersion-theory type formalism, and resonances are defined by the poles of an analytic continuation of the imaginary part of the reaction amplitude. The result is an ordinary Breit-Wigner type resonance, but it is obtained without the need for an "internal" Schrödinger equation with artificial boundary conditions at a "nuclear radius."

V-33-5 THE SUPERCURRENT STATE (ANL-6517, February-March 1962)

71

M. Peshkin . . . . . .

The model of Byers and Yang is extended to describe the current-carrying state in a thin superconducting ring, by including the magnetic interaction in the zero-order Hamiltonian. The induced magnetic field is treated self-consistently. Pairing degeneracy occurs for

PAGE

any value of the surrounded flux, but self-consistency is obtained only for quantized values of the flux.

V-38-1 PARTICLES WITH ZERO MASS AND PARTICLES WITH "SMALL" MASS (New project)

F. Coester 73

The irreducible representations of the inhomogeneous Lorentz group which describe respectively particles with and without mass are qualitatively different. Nevertheless, the zero-mass representations can be obtained from the representation with mass by letting the mass go to zero. Particles of sufficiently small mass or sufficiently high energy behave like particles of zero mass.

V-44-1 FOUNDATIONS OF QUANTUM MECHANICS (New project)

H. Ekstein 76

The basic postulate of quantum mechanics is the superposition principle. It has been felt by many, including this author, that a more directly verifiable, operational postulate would be more satisfactory. A new approach to the problem of "operational formulation of the foundations of quantum mechanics" is proposed here.

PUBLICATIONS 81

PERSONNEL CHANGES IN THE ANL PHYSICS DIVISION . . . 85

PROJECTS NOT REPORTED IN THIS ISSUE

A reference to the last preceding report is given in parentheses for each project.

I. EXPERIMENTAL NUCLEAR PHYSICS

I-2. Neutron Detectors (ANL-6534, April-May 1962), L. M. Bollinger and G. E. Thomas.

I-3. Cross-Section Measurements with the Fast Neutron Velocity Selector (ANL-6534, April-May 1962), L. M. Bollinger, R. E. Cote', H. E. Jackson, J. P. Marion, and G. E. Thomas.

I-7. Gamma-Ray Spectra from Capture in Neutron Resonances (ANL-6603, July-August 1962), H. E. Jackson.

I-11. Installation and Operation of the Van de Graaff Generator (ANL-6488, January 1962), J. R. Wallace.

I-18. Neutron Polarization and Differential Cross Sections (ANL-6666, November-December 1962), J. E. Monahan and A. J. Elwyn.

I-19. Nuclear Resonance Absorption of Gamma Rays (ANL-6603, July-August 1962), R. S. Preston, S. S. Hanna, and J. Heberle.

I-22. Scattering of Charged Particles (ANL-6574, June 1962), H. W. Broek and J. L. Yntema.

I-24. Studies of Pickup Reactions (ANL-6612, September-October 1962), B. Zeidman and T. H. Braid.

I-28. Angular Correlations in Charged-Particle Reactions (ANL-6358, April-May 1961), T. H. Braid.

I-30. Calculation of Reduced Widths from Resonant Scattering of Protons by a Diffuse Potential (ANL-6534, April-May 1962), J. P. Schiffer.

I-35. Decay of $_{57}La^{135}$ (19.5 hr) (ANL-6391, July-August 1961), S. B. Burson and H. A. Grench.

I-60. 7.7-Meter Bent-Crystal Spectrometer (ANL-6517, February-March 1962), R. K. Smither.

I-80. Molecular Beam Studies (ANL-6612, September-October 1962), W. J. Childs, J. Dalman, D. von Ehrenstein, and L. S. Goodman.

I-98. Unbound Nuclear Levels in the KeV Region (ANL-6574, June 1962), C. T. Hibdon.

I-102. Neutron Cross Sections by Self-Detection (ANL-6376, June 1961), J. E. Monahan and F. P. Mooring.

I-111. Semiconductor Detectors (ANL-6455, November-December 1961), T. H. Braid and J. T. Heinrich.

II. MASS SPECTROSCOPY

II-23. Sputtering Experiments in the Rutherford Collision Region (ANL-6488, January 1962), M. S. Kaminsky.

II-28. Kinetics of Chemical Reactions in the Gas Phase (ANL-6517, February-March 1962), J. Berkowitz and S. Wexler.

II-29. Gaseous Species in Equilibrium at High Temperatures (ANL-6666, November-December 1962), J. Berkowitz and J. R. Marquart.

II-39. Fragmentation of Cyanogen (ANL-6488, January 1962), H. E. Stanton.

II-41. Consecutive Ion-Molecule Reactions (ANL-6603, July-August 1962), S. Wexler.

IV. PLASMA PHYSICS

IV-10. Morphology of High-Frequency Plasmoids (ANL-6574, June 1962), A. J. Hatch.

V. THEORETICAL PHYSICS, GENERAL

V-2. Properties of Light Nuclei (ANL-6612, September-October 1962), D. Kurath.

V-3. Dynamics of Nuclear Collective Motion (ANL-6517, February-March 1962), D. R. Inglis.

V-4. Relative β-Decay Probabilities for $_{19}K^{40}$ (ANL-6455, November-December 1961), D. Kurath.

V-8. Relationships of Collective Effects and the Shell Model (ANL-6358, April-May 1961), D. Kurath.

V-9. Interpretation of Experiments Involving Excitation of the 15.1-MeV Level of C^{12} (ANL-6391, July-August 1961), D. Kurath.

V-15. Statistical Properties of Nuclear Energy States (ANL-6488, January 1962), N. Rosenzweig.

V-26. Preacceleration in Electron Theory (ANL-6603, July-August 1962), M. N. Hack.

V-39. Spin and Statistics with an Indefinite Metric (ANL-6603, July-August 1962), R. Spitzer.

V-42. Time Reversal and Superselection (ANL-6488, January 1962), H. Ekstein.

V-45. Meson-Nucleon Interaction (ANL-6666, November-December 1962), L. S. Liu and K. Tanaka.

V-46. Elastic Nucleon-Nucleon Scattering at High Energies and Small Angles (ANL-6517, February-March 1962), K. Hiida.

I. EXPERIMENTAL NUCLEAR PHYSICS

I-10-2 Tandem Van de Graaff Accelerator (51210-01)

1. INSTALLATION

Jack R. Wallace

The following is a chronological summary of the tandem Van de Graaff accelerator project of the Physics Division.

The first shipments of parts from the High Voltage Engineering Corporation began to arrive July 10, 1961. The Tandem wing on Building 203 (Fig. 1) was not accepted from the contractor until October 1961. The reassembly of the Tandem was slower than had been anticipated because of the condition of some of the equipment when received. The alignment of the equipment also required excessive amounts of time.

The acceptance tests of the accelerator (Sec. 2) were delayed until February 2, 1962 because of a "loading" problem in the

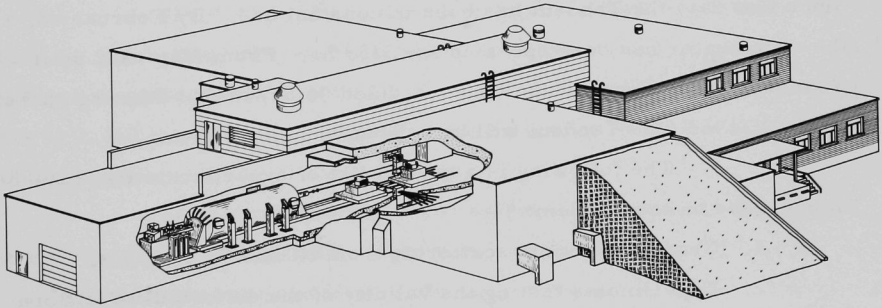

Fig. 1. Perspective drawing of the tandem wing of the Physics Building. The wing attaches to the Physics Building (not shown) along the upper right-hand side. The earth shielding (shown cut away) extends along the sides of the target rooms and almost to the end of the accelerator vault. See pp. 3-4 of ANL-6262 (Physics Division Summary Report, December 1960) for floor plans and vertical section.

accelerating tube, a troublesome discharge current when the voltage was raised. Installation of auxiliary vacuum systems in each target area, extension of the beam tubes, placement of shielding blocks in the walls between machine vault and target rooms, and the installation of experimental cables, interlocks, etc. had to be delayed until acceptance tests were completed by High Voltage Engineering.

The items mentioned above were completed during the month of February and the first preliminary experiments with the Tandem were started on March 5, 1962. This period of operation was merely to familiarize the experimenters and technicians with the operating of the machine.

Starting March 26, 1962, the Tandem was shut down while the new 90° analyzer magnets were installed. The original analyzer magnets supplied by High Voltage had a 28-in. radius of curvature and were designed to deflect ions for which the product of mass and energy could have values up to 36 amu-MeV. They had agreed to replace these magnets after the acceptance tests with magnets having a 34-in. radius of curvature for ions with $mE \leq 52$ amu-MeV.

Operation of the Tandem was again resumed on May 7, 1962. Since that date the Tandem has been in constant use. By February 5, 1963, the accelerator had been operated for 3335 hr. From May 1962 until February 1963, the machine was scheduled 96 hr/week. Starting on February 4, 1963, the Tandem will be scheduled 120 hr/week.

The following is a partial list of experiments that have been in progress on the Tandem:

1. Charged-particle scattering from Ni and Cu isotopes.
2. Experiments testing the validity of the distorted-wave Born approximation for $Ca^{40}(d, p)Ca^{41}$.
3. Measurements on $B^{10}(d, Li^{6})Li^{6}$.
4. $B^{11}(p, \gamma)C^{12}$.
5. $B^{10}(p, p'\gamma)B^{10}$.
6. Cross sections of α-particle reactions.

7. $Al^{27}(p, \alpha)Mg^{24}$.

8. $K^{39}(p, \alpha)Ar^{36}$.

Several large pieces of experimental equipment are now being installed in the target areas. One of these is a large remotely-operated scattering chamber designed by Jan Yntema. This chamber is being installed by the Central Shops. Preliminary work has been done for the installation of a broad-range magnetic spectrometer for John Erskine and Linwood Lee.

The acceleration of heavy ions is also being studied at the Tandem.

2. ACCEPTANCE TESTS

William Evans, Paul Mooring, John Schiffer, Ralph Segel, and Jack Wallace

Protons were used to demonstrate the performance ratings of the tandem; helium ions were used to demonstrate the performance ratings of the helium injector.

The $Al^{27}(p, n)Si^{27}$ threshold at 5.800 MeV was used to calibrate the generating voltmeter and to establish the magnet constant for both analyzer magnets. The object slits were set at 0.150 in. and the image slits at 0.050 in. These settings were maintained for all tests with a particular magnet.

The reproducibility of the analyzer magnets was checked by the $Fe^{54}(p, p'\gamma)Fe^{54*}$ reaction. Excitation curves were run first by increasing the magnet current from a low value and second by decreasing the magnet current from a very high value, the magnetic field in each case being measured by nuclear magnetic resonance. Shifts in the NMR frequencies at which the resonances in the gamma-ray yield occurred correspond to an energy shift of 1.8 keV for magnet No. 1 (Fig. 2) and a shift of 1.0 keV for magnet No. 2. The width of the resonances observed

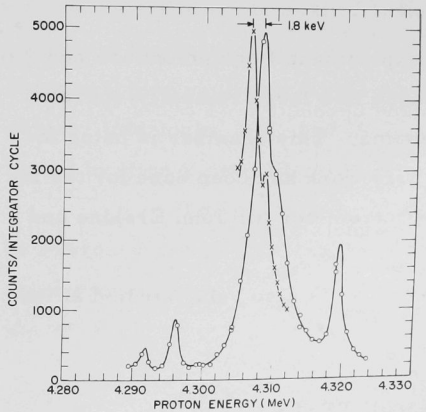

Fig. 2. Proton spectrum from the $Fe^{54}(p, p')Fe^{54*}$ reaction. These data were taken with a target approximately 1 keV thick. The target was in the west target room, into which it was deflected by magnet No. 1. Points marked by circles were taken when the proper magnet current (about 4 A) was reached by increasing from zero. Those marked x were taken after the magnet current had been raised to 12 A and then returned to the proper value.

in this reaction indicated that the energy spread of the system was less than ± 2 keV.

The $Fe^{54}(p, p'\gamma)Fe^{54*}$ reaction and the $Ni^{58}(p, n)$ threshold were used to check the calibration constant at widely divergent fields. The agreement was better than the known energy values for the two reactions. The energy stability of the over-all system was checked by sitting on the side of one of the sharp $Fe^{54}(p, p'\gamma)$ resonances and noting the time dependence of the counting rate. The energy drift during the course of this run was less than 500 eV.

The ion-beam current was measured in both target rooms at the end of the 15° beam line. It was measured in a Faraday cage biased at a potential of +300 V. A current exceeding 2.0 μa was observed during 1-hr runs at 3 MeV and at 6.5 MeV and during a 2-hr run at 10 MeV. During each of these six runs, the current exceeded 2.0 μa for more than 95% of the time.

The diameter of the ion beam was checked by observing the beam spot on a quartz viewer. At all energies and for all currents for which observations were made, the spot size was satisfactory. The positional stability of the ion beam also exceeded the contractual requirement (ion-beam diameter ≤ 5 mm, positional stability ± 2 mm).

The magnetic field of each analyzer magnet (rated for ions for which the product of mass and energy was 36 amu-MeV) proved more stable than specified.

All observations were made beyond the switching magnets.

The voltage calibration of the helium-ion injector was checked by using the $C^{13}(\alpha, n)O^{16}$ reaction. This also checked the performance of the analyzer and switching magnets at high fields. The voltage stability of the injector was better than the contract figure of ±50 keV during this run. An ion-beam diameter of less than 0.250 in. was observed on a quartz viewer.

Currents in excess of 1.5 μa He^{+} and 0.5 μa He^{++} were maintained for the proper times and at the appropriate energies. The energies of the helium-ion beam were checked by using the $C^{13}(\alpha, n)O^{16}$ reaction.

After installation, the large analyzer magnets designed for ions with a mass-energy product of 52 amu-MeV were checked against the $Fe^{54}(p, p'\gamma)Fe^{54*}$ resonances and found equally satisfactory.

I-14-24 Pulsed-Beam Experiments with the Van de Graaff Machine (51210-01)

F. J. Lynch and E. N. Shipley
Reported by F. J. Lynch

PULSED-BEAM MEASUREMENTS ON THE DOUBLET IN Se^{77}

Robinson, McGowan, and Stelson[1] proved that what was once thought to be a single excited state in Se^{77} near 245 keV was, in fact, two closely spaced levels. Figure 3 shows the energy-level diagram with the energies and spins assigned by them to these levels. The lower level at

---

[1] R. L. Robinson, F. K. McGowan, and P. H. Stelson, Phys. Rev. 125, 1373 (1962).

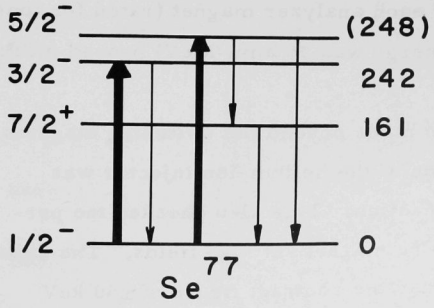

Fig. 3. Energy-level diagram for the lower levels of Se^{77}, as reported by Robinson, McGowan, and Stelson (reference 1).

242 keV is strongly excited by Coulomb interaction and decays to the ground state by a mixture of E2 and M1 transitions. The upper level is weakly excited and decays to the ground state by an E2 transition or to the first excited state by an E1. Prior to the general recognition that there was a doublet, there were two direct lifetime measurements attributed to the 245-keV level. Using Coulomb excitation with pulsed He ions on a normal Se target, Holland and Lynch[2] measured a mean life of 0.1 nsec. This undoubtedly referred to the lower level at 242 keV, which strongly dominates in Coulomb excitation. Later, T. D. Nainan,[3] using gamma-gamma delayed coincidence techniques with a Br^{77} source, reported a mean life of 1.9 nsec. Robinson, McGowan, and Stelson assumed that that this was associated with the upper level at 249 keV. Since Holland and Lynch had observed a weak unidentified gamma ray with a lifetime longer than reported, we undertook to measure the lifetime of the upper level and the relative intensities of the gamma rays, using pulsed-beam techniques with an enriched Se^{77} target.

The target was a thick layer of Se^{77} (enriched to 74%) evaporated on copper. The measurements were made with an externally pulsed beam of singly charged He^4 ions at from 2.6 — 3.5 MeV from the electrostatic accelerator. The detector was a NaI(Tl) scintillator

---

[2] R. E. Holland and F. J. Lynch, Phys. Rev. 121, 1464 (1961).

[3] T. D. Nainan, Phys. Rev. 123, 1751 (1961).

oriented first at 0° and later at 125° relative to the ion beam. The nuclear states were excited by Coulomb interaction with short bursts of ions, and the time of emission of the various de-excitation gamma rays was observed relative to the time of the burst. The equipment and techniques have been described previously.[2,4,5]

Figure 4 shows the normal scintillation pulse-height spectrum observed with alpha particles on Se^{77}. The prominent large photopeak at 242 keV corresponds to the ground-state transition from the lower level of the doublet. There is no evidence of the ground-state transition from the upper level. The small photopeak at about 87 keV was shown by Robinson et al.[1] to be due to the transition from the upper level to the first excited state. When we look at the time of occurrence of the gamma rays producing these two photopeaks, we obtain the time spectra shown in Fig. 5. This shows the unaltered time spectra of the gamma rays in the entire photopeaks at around 87 keV and around 242 keV. Both spectra show a fast component followed by a slow component and provide a measure of the lifetimes of the two levels. In addition to measuring the lifetimes, the time spectrum of the 242-keV gamma rays was used to obtain the relative intensities of the ground-state transition from the two levels.

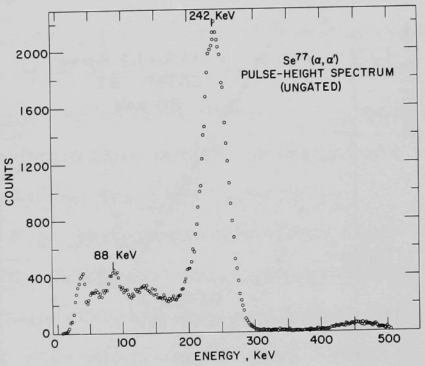

Fig. 4. Ungated scintillation pulse-height spectrum from a Se^{77} target bombarded with 3.0-MeV alphas. Detector is a NaI(Tl) cylinder $\frac{1}{2}$ in. thick by 1 in. in diameter.

---

[4] R. E. Holland, F. J. Lynch, and S. S. Hanna, Phys. Rev. 112, 903 (1959).

[5] F. J. Lynch and R. E. Holland, Phys. Rev. 114, 825 (1959).

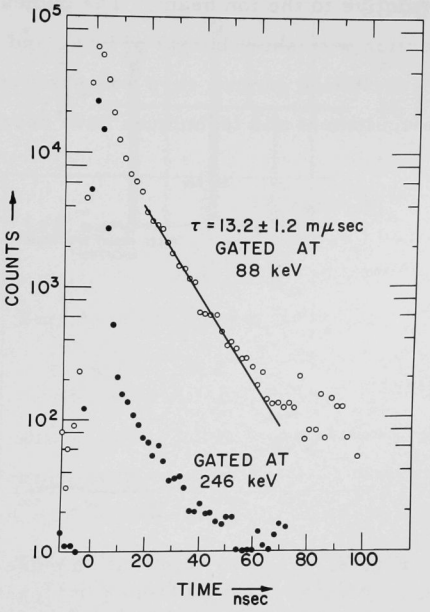

Fig. 5. Time spectra of Se^{77} gamma rays. The upper curve (open circles) was taken with a broad energy gate centered around 90 keV, the lower (solid circles) with a broad gate centered around 246 keV.

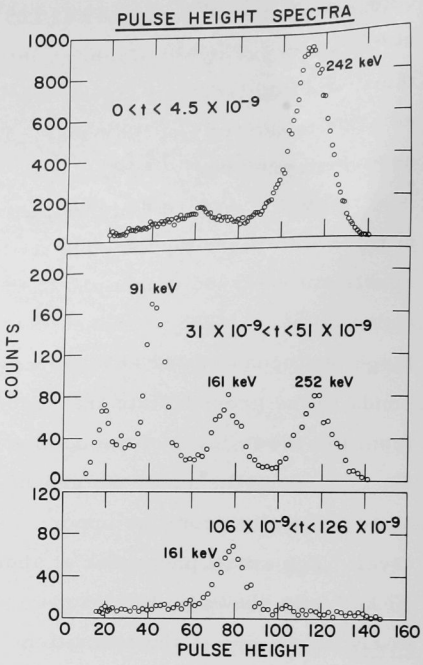

Fig. 6. Scintillation pulse-height spectra obtained at different times after the formation of the excited states in Se^{77}. The upper curve shows the spectrum associated with the fast component, the middle curve that associated with the slow component, the lower curve that associated with the random component (very long times).

Since the experiment yields time spectra as well as energy spectra, it is convenient to look at the pulse-height spectrum which is in coincidence with a specific interval of time. Figure 6 shows such spectra. The upper curve shows the spectrum associated with very short intervals after the time of the ion burst. This shows one photopeak at 242 keV due to the ground-state transition from the lower level. The middle curve shows the pulse-height spectrum taken after the fast component has decayed but before the slow component has completely

decayed. It shows a photopeak at 249 keV due to the ground-state transition from the upper level. Another photopeak at 88 keV corresponds to the transition from the upper level to the first excited state. The middle photopeak at 161 keV is due to the decay of the first excited state which has a lifetime of 17.5 sec. The lower spectrum was taken at a time after the slow component had completely decayed and shows only the photopeak at 161 keV due to the decay of the long-lived first excited state. It was used for subtracting background from the spectrum associated with the slow component. From these spectra, one may obtain the energies of the gamma rays and the branching ratio of the transitions from the upper level.

From the time spectra (Fig. 5) the mean life of the slow component was obtained by measuring the reciprocal slope at times after the fast component had decayed. The value obtained from such measurements was $\tau = 13.2 \pm 1.2$ nsec for the mean life of the 249-keV level. In order to measure the mean life of the fast component, it is necessary to subtract the slow component from the spectrum. The difference is a pure fast spectrum which can then be compared with the spectrum of a prompt gamma ray of the same energy. To do this, the IBM-1620 computer was first used to generate the pure time spectrum D(T) to be expected for a gamma ray with a lifetime $\tau = 13.2$ nsec by use of the convolution integral

$$D(T) = \int_0^T P(T - t)e^{-t/\tau}\, dt,$$

where P(t) is the measured prompt spectrum. Then, after the amplitude of D(t) was adjusted to fit the tail of the measured spectrum, it was subtracted from the measured spectrum. The resultant pure fast spectrum was then compared with a prompt time spectrum which was taken at the same energy by using a narrow window at 242 keV on part of the Compton distribution from the 480-keV gamma ray ($\tau \approx 10^{-13}$ sec) from a Li^7 target. The mean life of the 242-keV level was calculated from the centroid shift to be 0.070 ± 0.05 nsec. When the previous lifetime data[2] are cor-

rected for the presence of the slow component, they yield $\tau = 0.075 \pm 0.05$ nsec in good agreement. The errors indicated are partly due to erratic fluctuations in the measurements but are mostly due to systematic errors generally encountered, but only qualitatively understood.[2] The calculation also yielded the ratio of the fast component to the slow one, thereby giving the relative intensities of the ground-state transitions from the two levels in the doublet. For the latter measurement, a broad window was used which more than covered the photopeak. In order to minimize excitation of the 242-keV level by cascade from the 440-keV level, the above data were taken with a bombarding energy of only 2.6 MeV.

From the time-gated spectra similar to those shown in Fig. 6, the energies of all the gamma rays and the branching ratio of the gamma rays from the upper level were obtained. From the relative counts in the photopeaks, the relative gamma-ray yields were obtained after the following corrections were made.

1. The probability that a gamma ray would be totally absorbed in the crystal was calculated by use of a Monte Carlo calculation of Miller and Snow[3] on the IBM-704. This was carried out for the scintillator and geometric arrangement at the gamma-ray energies of interest.

2. A correction was made for absorption in the target assembly and scintillator window.

3. A correction was made for the shift of the centroid of the time spectrum of a prompt gamma ray as the gamma-ray energy changes. This energy dependence is due to the time constant in the scintillator. The correction was calculated in two ways. The simpler way consists of applying a correction factor $e^{-\overline{\Delta t}/\tau}$ to the yield of 88-keV gamma rays, where the energy-induced time shift is $\overline{\Delta t} = \overline{t}_{88} - \overline{t}_{249}$, in which $\overline{t}_{88}$ is the centroid of the prompt spectrum at 88 keV, $\overline{t}_{249}$ is the centroid of the prompt spectrum at 249 keV, and τ is the mean life of the 249-keV level. A more

---

[3] W. F. Miller and W. J. Snow, Rev. Sci. Instr. 31, 39 (1960).

careful calculation was made by generating (as described above) the time spectra for τ = 13.2 nsec by use of measured prompt spectra taken at 88 keV and 249 keV. This is shown in Fig. 7, which also shows the positions of the windows for the middle and lower pulse-height spectra in Fig. 5. From these curves, the number of counts in each window was obtained for each energy; and the correction was calculated. The results were nearly the same as in the simpler calculation.

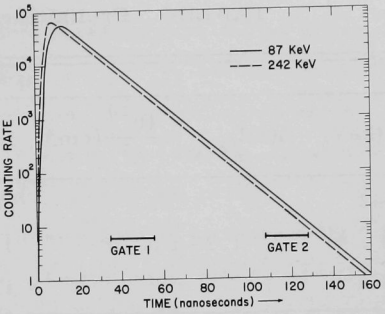

Fig. 7. Time spectra, calculated with the convolution integral, for gamma rays whose mean life is 13.2 nsec and whose energy is 87 keV or 242 keV.

4. No correction was made for the angular distribution of the gamma rays from the 249-keV level. To speed data accumulation, most of the data on this level were taken with the detector in the forward direction where it subtended a solid angle of π radians. If the initial orientation of the excited nucleus were maintained until gamma rays were emitted, one would expect the intensity of the 249-keV gamma ray to be 9% greater in the forward direction than at 125°. Experimentally, it was found that the intensity was about 10% higher at 125°. This is probably not significant, however, because the experiments were performed at different times with different detectors.

5. Robinson et al.[1] found $A_2 = 0.00 \pm 0.12$ for the 88-keV gamma ray and $A_2 = -0.085 \pm 0.028$ for the 242-keV gamma. To correct for this asymmetry in the angular distribution of the 242-keV gamma rays, the intensity measured in the forward direction must be reduced by 2.5%.

The preliminary results are listed in Table I. The energy measurements are in good agreement with those of Robinson et al.[1], although the technique employed should permit more accuracy than we

TABLE I. Preliminary results of measurements.

Se^{77}				
E_γ (keV)	$B(E2)_{exc} \times \frac{10^{50}}{e^2}$ (cm^4)	τ (nsec)	I_{242}/I_{252}	I_{91}/I_{252}
242		0.07 ± 0.05	26.8 ± 3	0.48 ± 0.12
249 ± 4	1.25 ± 0.20	13.2 ± 1.2		
88 ± 3		13.2 ± 1.2		

Revised results of Robinson, McGowan, and Stelson

E (keV)	$B(E2)_{exc} \times \frac{10^{50}}{e^2}$ (cm^4)	$B(E2)_d/B(E2)_{sp}$	τ (nsec)
242	17.4 ± 1.5	45.4	0.035 ± 0.17
249	1.38 ± 0.50	2.16	

are able to report here. The branching ratio I_{88}/I_{249} from the 249-keV level is 0.48 ± 0.08. The relative intensity of the ground-state transitions of the doublet is $I_{242}/I_{249} = 27 \pm 3$. The mean life of the 249-keV level is 13.2 ± 1.2 nsec. That of the lower level is 0.075 ± 0.05 nsec. From the lifetime and branching ratio of the 249-keV level, B(E2) for excitation was calculated to be 1.25×10^{50} e^2cm^4.

Our results are in gross disagreement with the values of Robinson et al.[1] for the gamma-ray intensity ratios I_{88}/I_{249}, I_{242}/I_{249}, and the B(E2) for excitation for the 249-keV level, because their values are based on the wrong value for the lifetime of the 249-keV level. When the proper mean life τ = 13.2 nsec is used with their yield data, $B(E2)_{exc}$ for the 249-keV level is calculated to be $(1.38 \pm 0.5) \times 10^{-50}$ e^2cm^4, in

reasonable agreement with the independent measurement quoted above. Similarly, their value for the branching ratio I_{88}/I_{249} becomes 0.367, and I_{242}/I_{249} becomes 18 in fair agreement with our measured value. On the basis of their measured yield and our measured relative intensities, the $B(E2)_{exc}$ for the 242-keV level is reduced from 18.23 to 17.4×10^{-50} $e^2\,cm^4$. The indirect lifetime measured by them is thereby slightly increased to 0.035 ± 0.017 nsec. Our directly measured value is about double this, but the lower value is more probable because of its lower quoted error.

I-21-10 Excited States of Light Nuclei (51210-01)

J. A. Weinman

DETERMINATION OF LEVEL WIDTHS BY ELASTIC SCATTERING FROM THICK TARGETS

In the analysis of elastic-scattering experiments, one frequently seeks to determine whether or not observed differential cross sections are compatible with those derived from dispersion theory. When using solid targets whose thickness (in energy units) cannot readily be made less than the resonance width Γ, the energy spread introduced by target thickness, beam straggling, and the energy spread of the incident beam tend to spread the resonance. All of these factors may be combined and represented either by a square or Lorentzian function with an effective thickness T. This thickness T can be estimated from the observed widths of narrow resonances with $\Gamma \ll T$. This note indicates the effect of this spreading on the magnitude of a resonance, i.e., the difference between the maximum and minimum value of the cross section. It can thus be used to obtain an estimate of the value of Γ when $\Gamma < T$, provided that the resonance shape can be derived from dispersion theory and that one can make an estimate of the density distribution in the target. If other reactions

compete with the elastic scattering, and the total width Γ has been measured in another reaction, this procedure can be used to determine the ratio $\Gamma_{a\ell}/\Gamma$, where $\Gamma_{a\ell}$ is the partial width for the particle scattered elastically.

The differential cross section for elastic scattering may be derived from dispersion theory for well-isolated levels. The elastic-scattering cross section represents interference between Coulomb scattering, nonresonant nuclear scattering, and resonant scattering. This interference produces a myriad of resonance shapes.[1] The theoretical expressions may be approximated by Haeberli's expression

$$k^2 \frac{d\sigma}{d\omega}(\epsilon) = A + B \sin^2(2\zeta + \gamma), \tag{1}$$

where

$$A = k^2 \frac{d\sigma}{d\omega}(\epsilon_1)\Bigg|_{\text{minimum}}, \qquad A + B = k^2 \frac{d\sigma}{d\omega}(\epsilon_2)\Bigg|_{\text{maximum}}.$$

The slowly varying nonresonant data fix γ through the relations

$$A + B \sin^2\gamma = k^2 \frac{d\sigma}{d\omega}(\epsilon)\Bigg|_{\text{Rutherford + nonresonant}}$$

and

$$\zeta = \tfrac{1}{2} \tan^{-1}\left[\tfrac{1}{2}\Gamma/(E' - \epsilon)\right].$$

When spread by an effective square function corresponding to thickness T, the observed differential cross section will be

---

[1] H. T. Richards in Nuclear Spectroscopy, edited by F. Ajzenberg-Selove (Academic Press, New York, 1960), Vol. I, p. 127.

$$\overline{\frac{d\sigma}{d\omega}(E)} = \frac{1}{T}\int_{E-\frac{1}{2}T}^{E+\frac{1}{2}T} \frac{d\sigma}{d\omega}(\epsilon)\, d\epsilon = \frac{A}{k^2} + \frac{B}{k^2}\sin^2\gamma \qquad (2)$$

$$+ \frac{B\Gamma}{2Tk^2}(\cos 2\gamma)\left\{\arctan\frac{2(E'-E)+T}{\Gamma} - \arctan\frac{2(E'-E)-T}{\Gamma}\right\}$$

$$+ \frac{B\Gamma}{4Tk^2}(\sin 2\gamma)\log\left\{\frac{\Gamma^2 + [2(E'-E)+T]^2}{\Gamma^2 + [2(E'-E)-T]^2}\right\} .$$

The ratio R, defined as

$$R \equiv \frac{\overline{\frac{d\sigma}{d\omega}(E_1)}\Big|_{max} - \overline{\frac{d\sigma}{d\omega}(E_2)}\Big|_{min}}{\frac{d\sigma}{d\omega}(\epsilon_1)\Big|_{max} - \frac{d\sigma}{d\omega}(\epsilon_2)\Big|_{min}} \qquad (3)$$

$$= \frac{k^2}{B}\left(\overline{\frac{d\sigma}{d\omega}(E_1)}\Big|_{max} - \overline{\frac{d\sigma}{d\omega}(E_2)}\Big|_{min}\right) ,$$

is plotted in Fig. 8 as a function of T/Γ with γ as parameter.

If a Lorentzian function of the form

$$\frac{T}{2\pi} \cdot \frac{1}{(\epsilon - E)^2 + \frac{1}{4}T^2}$$

is assumed to describe the effective density distribution of the target, then

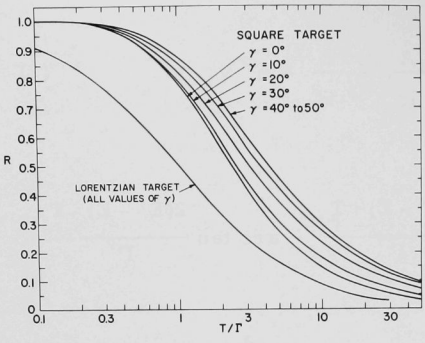

Fig. 8. The magnitude of a resonance, defined as the difference between the maximum and minimum value of the cross section, is spread by a thick effective target. Target thickness is given in units of resonance width. The curves are given for effective targets with square and Lorentzian density distributions.

$$\overline{\frac{d\sigma}{d\omega}(E)} = \frac{T}{2\pi k^2} \int_{-\infty}^{\infty} \frac{[A + B \sin^2(\gamma + 2\zeta)]}{(\epsilon - E)^2 + \frac{1}{4}T^2} d\epsilon \ . \qquad (4)$$

This expression was numerically integrated to find the spreading ratio R defined in Eq. (3). Figure 8 also includes a plot of R as a function of T/Γ for the Lorentzian function.

It will be noted that R has the same value for γ, $90^\circ - \gamma$, $90^\circ + \gamma$, and $180^\circ - \gamma$ when the resonance is spread by a square target, and that R is independent of γ when the resonance is spread by a Lorentzian target.

The shapes of the resonances spread by these functions retain the same qualitative features as the resonances derived from dispersion theory. However, distortions are introduced if the target is nonuniform.

The following isolated resonances in Si^{28} serve to illustrate the reliability of this method for determining the ratio $\Gamma_{a\ell}/\Gamma$ from elastic-scattering resonances spread by a thick target. Since the $Mg^{24}(a, p)Al^{27}$ reaction could compete with the elastic-scattering process, it was possible to determine the ratio $\Gamma_{a\ell}/\Gamma$ only for resonances for which Γ was known from radiative-capture reactions. Although the resonances in

Si^{28} which were studied by $Mg^{24}(\alpha,\alpha)Mg^{24}$ elastic scattering were also observed in the $Mg^{24}(\alpha,\gamma)Si^{28}$,[2] $Al^{27}(p,\gamma)Si^{28}$,[3] $Mg^{24}(\alpha,p)Al^{27}$,[4] and $Al^{27}(p,\alpha)Mg^{24}$[5] reactions, the parameters of only two resonances were sufficiently redundant to allow a comparison between the value of $\Gamma_{a\ell}/\Gamma$ derived by this method and $\Gamma_{a\ell}/\Gamma$ obtained from other measurements.

The differential cross section for elastic scattering was determined graphically[1] for various ratios $\Gamma_{a\ell}/\Gamma$. The quantum-mechanical expression for the elastic scattering of alpha particles by Mg^{24} (spinless particles on spinless nuclei) is given in the one-level approximation[6] by

$$\frac{d\sigma}{d\omega}(\epsilon) = k^{-2} \left| -\frac{a}{2} \csc^2\left(\frac{\theta}{2}\right) \exp\left[ia \ln \csc^2\left(\frac{\theta}{2}\right)\right] + \sum_{\ell=0}^{\infty} (2\ell+1) e^{2i(\eta_\ell - \eta_0)} \left\{ \frac{\Gamma_{a\ell}}{\Gamma} \sin(2\zeta + \zeta_\ell) \times \exp[i(2\zeta + \zeta_\ell)] \right\} P_\ell(\cos\theta) \right|^2 . \quad (5)$$

---

[2] P. J. M. Smulders and P. M. Endt, Physica 28, 1093 (1962); J. A. Weinman, L. Meyer-Schützmeister, L. L. Lee, Jr., and S. S. Malik, Bull. Am. Phys. Soc. 7, 73 (1962).

[3] S. L. Andersen, H. Bö, T. Holtebekk, O. Lönsjö, and R. Tangen, Nuclear Phys. 9, 509 (1958/59).

[4] S. G. Kaufmann, E. Goldberg, L. J. Koester, and F. P. Mooring, Phys. Rev. 88, 673 (1952).

[5] S. L. Andersen, A. Haug, T. Holtebekk, O. Lönsjö, and R. Nordhagen, Physica Norvegica 1, 1 (1961).

[6] R. G. Sachs, Nuclear Theory (Addison-Wesley Press, Cambridge, 1953).

Here k is the relative wave number; $a = Z'Z''e^2 M/\hbar^2 k$, where Z' and Z'' are the charges of the target and projectile, and M is the reduced mass of the alpha-Mg^{24} system; θ is the center-of-mass scattering angle;

$$e^{2i(\eta_\ell - \eta_0)} = \prod_{t=1}^{\ell} \left(\frac{t + ia}{t - ia}\right) ;$$

$\Gamma_{a\ell}$ is the partial width for alphas from the level E_r of the compound nucleus; and $\Gamma = \sum_s \Gamma_s$, where s runs over all open channels.

The resonant phase shift is

$$\zeta = \tfrac{1}{2} \tan^{-1} \left[\tfrac{1}{2}\Gamma/(E' - \epsilon\right] .$$

Here $E' = E_r + \frac{1}{2}\sum_s Q_{ss}\,\Gamma_s$, where $Q_{ss} = -F_s(a_{0s})/G_s(a_{0s})$, with F_s and G_s defined in reference 6. [These functions differ from the usually tabulated functions by a factor $(M_s/\hbar k)^{\frac{1}{2}}$.]

The potential phase shift is $\zeta_\ell = \tan^{-1} Q_{\ell\ell}$, with $Q_{\ell\ell} = -F_\ell(a_{0\ell})/G_\ell(a_{0\ell})$. Here F_ℓ and G_ℓ are the regular and irregular Coulomb functions defined in reference 6.

Haeberli's approximation (1) was then fitted to the theoretical cross section (5). The observed widths of the narrow resonances in the elastic-scattering experiment were assumed to be entirely due to target thickness and straggling in an excessively thick target (T = 13 keV). The square density-distribution function was assumed applicable to this analysis. The ratio $\Gamma_{a\ell}/\Gamma$ could then be determined from the values of T, Γ, γ, and R by means of Fig. 8.

Table II compares the results of this procedure for deter-

mining $\Gamma_{a\ell}/\Gamma$ with this ratio derived from other measurements.

The present method displays somewhat greater internal consistency for resonances with widths Γ exceeding 2 keV than for the narrow resoances cited in Table II.

TABLE II. Comparison of $\Gamma_{a\ell}/\Gamma$ from elastic scattering with the value from other measurements.

$E_{a\,lab}$(MeV)	ℓ^{π}	Γ(keV)	$\Gamma_{a\ell}/\Gamma$(elastic)	$\Gamma_{a\ell}/\Gamma$ (other)
3.213 ± 0.007	2^+	0.71 ± 0.13[a]	0.4 ± 0.2	0.6[b]
3.418 ± 0.007	2^+	≈ 1.1[c]	0.3 ± 0.2	0.5[c]

[a]Reference 3.
[b]Reference 2.
[c]Reference 5.

I-27-1 Studies of Deuteron-Induced Reactions (51210-01)

J. P. Schiffer, L. L. Lee, Jr., and B. Zeidman

A STUDY OF THE Ca(d, d)Ca AND Ca^{40}(d, p)Ca^{41} REACTIONS

In recent years the Distorted-Wave Born Approximation (DWBA) has been used to obtain theoretical fits to experimental results from stripping and pickup reactions. Our present experiment is intended to test the theory's predictions of absolute cross sections and shapes of angular distributions over a range of deuteron energies. Preliminary results are reported here.

The Ca^{40}(d, p)Ca^{41} reaction was chosen for study because some of the low-lying final states in Ca^{41} are believed to be very nearly good single-particle states. In particular, the Ca^{41} ground state should

contain the entire $1f_{7/2}$ stripping width and excited states at 1.95, 2.45, and 3.95 MeV should contain almost the full p-wave width, with the $1p_{3/2}$ strength concentrated in the state at 1.95 MeV excitation. In this case then, the "spectroscopic factors" for the (d, p) reaction can be assumed to be known so that the DWBA can be used to predict exact absolute cross sections.

The DWBA calculations use an optical potential to describe the distortion of the incident wave by the nucleus. It is necessary, therefore, to first measure the elastic deuteron scattering from the nucleus under investigation and use these results to obtain parameters for an optical potential. These parameters can then be used, without further fitting, in DWBA calculations to predict the differential cross sections for the (d, p) reaction. The feasibility of this approach is then indicated by the fit between these predictions and the observed experimental results.

We have used the deuteron beam from the Argonne tandem Van de Graaff generator to bombard natural Ca targets at deuteron energies of 7.0, 8.0, 9.0, 10.0, 11.0, and 12.0 MeV. Semiconductor counters were used to detect the reaction protons and elastically scattered deuterons. The targets were thin rolled foils of natural Ca about 60 keV thick to the deuteron beam. Measurements were made over an angular range from 10° to 168°. Absolute cross sections were obtained from comparison with the Coulomb scattering of 4-, 5-, and 6-MeV alpha particles in the same geometric arrangement.

The results for the elastic deuteron scattering, plotted relative to the cross section for Rutherford scattering, are shown in Fig. 9. Except where shown, the errors are of the order of the size of the points. The absolute cross sections are believed to be accurate to about 5%. Proton angular distributions were measured for the four most prominent groups from Ca^{41}, corresponding to Q values of 6.14, 4.19, 3.67, and 2.19 MeV. The measured differential cross sections for the Q = 6.14 and 4.19 MeV groups are shown in Figs. 10 and 11, respectively. Here

the absolute cross sections are believed accurate to 10% or better. We expect to improve this precision with further measurements.

G. R. Satchler and his collaborators at Oak Ridge National Laboratory are now analyzing the above data. Preliminary results for the elastic deuteron scattering have yielded several sets of parameters for the optical potential that give approximately equally good fits to the measured differential cross sections. There is usually no smooth variation of of these parameters with energy. In particular, the best-fit radius of the potential well changes by as much as 30% from 8 to 12 MeV. Also, all of the radii that give good fits are unusually small, with R_0 of the order of 1.0 fermi.

The theoretical predictions for the (d, p) differential cross sections obtained from the preliminary sets of optical

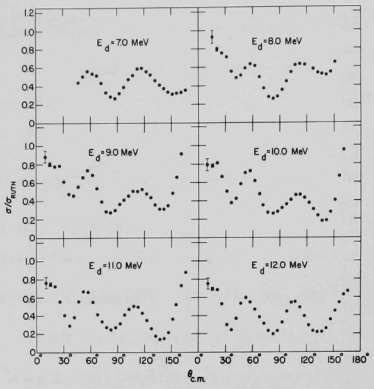

Fig. 9. Elastic scattering of deuterons from Ca, plotted relative to the Rutherford cross section for the laboratory energies indicated. The thin Ca foil target was about 60 keV thick to the incident deuterons.

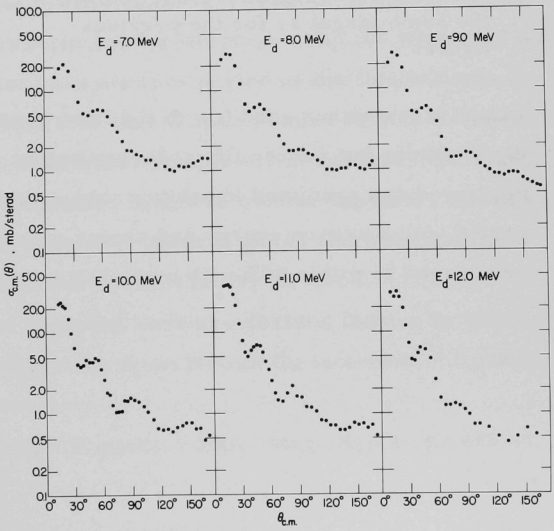

Fig. 10. Center-of-mass differential cross sections for the Q = 6.14 MeV group from the $Ca^{40}(d, p)Ca^{41}$ reaction. The target is the same as used for Fig. 9.

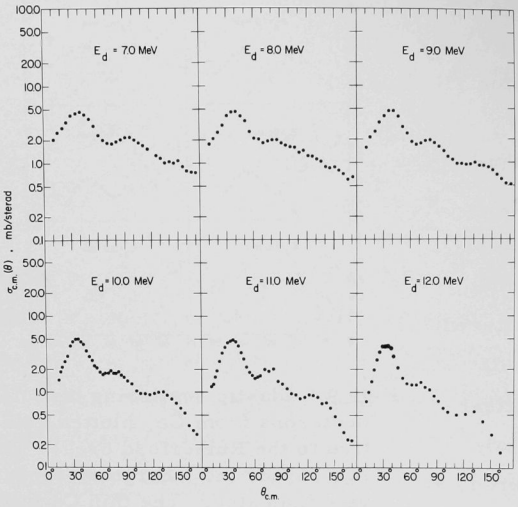

Fig. 11. Center-of-mass differential cross sections for the Q = 4.19 MeV group from the $Ca^{40}(d, p)Ca^{41}$ reaction with the same target as for the previous figures.

parameters have been calculated for the Q = 6.14 MeV and Q = 4.19 MeV groups. In these calculations the Q = 6.14 MeV group was assumed to contain the entire $1f_{7/2}$ stripping width and the Q = 4.19 MeV group was assumed to contain the entire $2p_{3/2}$ stripping width. When no cutoff is used for the radial integration, the fits to the measured results are usually very poor both in shape and absolute cross section. Introduction of a cutoff at about the nuclear radius gives rather good fits to the first maxima of the proton angular distributions but poorer fits at larger angles. The agreement between the measured and predicted absolute cross sections on the stripping maximum varied with deuteron energy and choice of potential. On the average, the two agreed to within 30% with much better agreement in some cases.

I-31-3 Elastic Scattering of Protons (51210-01)

L. L. Lee, Jr. and J. P. Schiffer
Reported by J. P. Schiffer

A TEST OF THE STATISTICAL NATURE OF FLUCTUATIONS IN NUCLEAR CROSS SECTIONS

The statistical fluctuation of nuclear cross sections has been discussed in some detail by Ericson.[1] His discussion depends strongly on the detailed validity of the statistical assumption that levels are spaced randomly and furthermore that the widths of levels are also distributed at random. It is the purpose of this note to point out that this assumption does not seem to be valid in at least two cases in which compound nuclei with $A \approx 60$ were excited to energies of 10—15 MeV. The assumption of a random distribution implies that the observed fluctuations of an experimental cross section as the energy changes will be inversely proportional to the square root of the experimental resolution width ΔE whenever ΔE is comparable to or greater than the true period of the fluctuations.

It is clear that this rule will be obeyed only if the levels in the compound nucleus are distributed completely at random. If there is any tendency for strongly populated levels to cluster together, as may occur in some cases,[2] one may well observe gross fluctuations which are in fact not the statistical ones discussed by Ericson.

The results reported here are derived from a detailed study of the elastic scattering of protons from Ni and Cu isotopes.[3] Excitation

---

[1] T. Ericson, "Advances in Physics," Phil. Mag. Suppl. 9, 425 (1960).

[2] A. M. Lane, R. G. Thomas, and E. Wigner, Phys. Rev. 98, 693 (1955).

[3] L. L. Lee, Jr., J. P. Schiffer, and J. R. Erskine, Bull. Am. Phys. Soc. 7, 532 (1962).

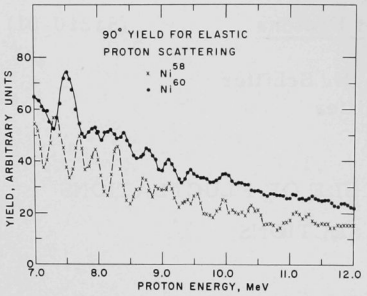

Fig. 12. Excitation function at 90° of the elastic scattering of protons from Ni^{58} and Ni^{60}. The target thickness was 3.32 mg/cm^2 for Ni^{58} and 5.06 mg/cm^2 for Ni^{60}, approximately 100 and 150 keV.

functions for the 90° scattering from Ni, shown in Fig. 12, indicate that the cross sections do in fact fluctuate, seemingly with periods which are 2 to 3 times the experimental resolution widths. Ericson's paper considered only reaction cross sections. As long as one is considering only the periods of fluctuations or their relative amplitudes, however, it is clear that the statistical treatment will apply equally well to elastic scattering. It is only in the absolute magnitude of the fluctuations that the nonresonant potential and Rutherford scattering will play a role, similar to the role of direct components in reactions.

An examination of Fig. 12 with a knowledge of the target thickness would lead one to conclude that the mean width of the levels is about 250 keV and thus one would be led to conclude that the so-called "lifetime of the compound system" is of the order of 2×10^{-21} sec. Figure 13 shows two excitation functions of the proton scattering from Ni^{58}, one taken with a resolution width of 6 keV and the other with 120 keV. It is clear that while the lower curve appears to show about one and a half resonances the upper curve indicates that this structure is in fact caused by many narrow resonances with widths of 8 — 15 keV or less. It is clear that the estimate of the lifetime would have been in error by at least a factor of 20.

The next quantity one can compute is the r.m.s. fluctuation in the cross section. Since the energy interval is small, the contribution of the energy variation of the nonresonant scattering can be assumed to be negligible. If one assumes (as is indicated by the data) that the true

average width of the fluctuations is equal to or less than 6 keV, the expected ratio of the r.m.s. fluctuations would be $\sqrt{125/6} \approx 4.5$ or larger. The actual r.m.s. deviations were 33.3% and 16.75% so their ratio is 2.0. In other words, one would have expected that a twenty-fold increase in the experimental resolution width would have decreased the observed fluctuations by a factor of 4.5. The fact that the fluctuations are only decreased by a factor of two indicates that in this case the compound nucleus is not well represented by the complete randomness of the statistical model but that some residual interactions cause clustering of strong levels which in turn give rise to gross fluctuations. The lifetime that would be deduced from the periods of these gross fluctuations is in fact indicative of the lifetime of a corresponding simple configuration in nuclear matter. Whether these are simply the single-particle states of Lane, Thomas, and Wigner or slightly more complicated configurations is not entirely clear.

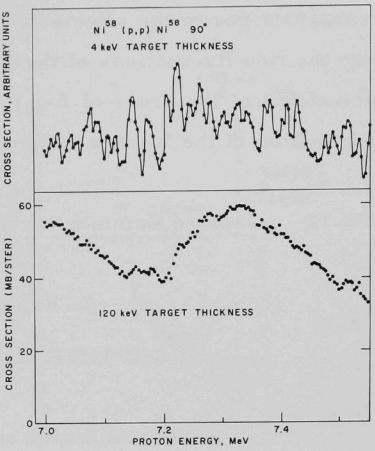

Fig. 13. Excitation function at 90° of the elastic scattering of protons from Ni^{58} between incident-proton energies of 7.0 and 7.5 MeV. The upper curve was taken with a target thickness of 4 keV and an experimental resolution of 6—7 keV. The lower curve was taken with the same target as the one used in Fig. 12. It was about 120 keV thick.

Similar results have been obtained at the higher bombarding energies and also in the fluctuations of the proton-scattering cross section for Ni^{60}. It is clear that the assumption of complete randomness, which is basic to the statistical model, is invalid in these cases. It would seem that experimental data must be treated with great care if the gross

fluctuations due to the effects of nuclear structure are to be distinguished from the fine fluctuations of the type discussed by Ericson. Observed fluctuations of the order of 2 — 3 times the experimental resolution width may well be of the former rather than the latter kind.

I-55-12 Capture Gamma-Ray Spectra for Neutrons with Energies from 0.1 to 10 eV (51210-01)

S. Raboy and C. C. Trail

CAPTURE GAMMA RAYS FROM Ca^{44}

Two scintillation counters of NaI(Tl) with anticoincidence annuli of NaI(Tl) are used to study the capture gamma rays from Ca^{44}. Both counters are buried within a massive shield, Fig. 14, which consists of concentric cylinders of paraffin (6 in. thick), and boron carbide (1 in. thick), lead (9 in. thick inside a steel cylinder 1 in. thick), and finally each counter has its own cylindrical shield of lithium carbonate. The neutron beam enters a slotted channel perpendicular to the axis of the cylinder and strikes a target in the channel placed on the axis of the cylinder. The slotted channel is lined with boral. Immediately in front of each counter is a lead cylinder, 2 in. thick and 10 in. in diameter with a hole in the center with a diameter of 1.5 in. Between the lead and the target is placed a shield of lithium carbonate enriched to 95% Li^6. The Li^6 shield is 1 in. thick.

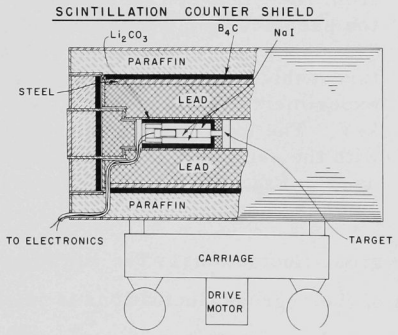

Fig. 14. Shield for scintillation counter.

This system of shielding makes possible the study of capture gamma rays in materials with very low absorption cross section.

Figure 15 is the spectrum obtained from a graphite target. The gamma rays from the $C^{12}(n,\gamma)C^{13}$ reaction are seen easily. It should be noted that the capture cross section in C^{12} is 3 mb.

The calcium sample enriched in Ca^{44} was placed in the beam and observations were made on the capture gamma rays. Figure 16 shows a singles spectrum of Ca^{44}. More than 20 gamma rays are seen. Preliminary energy determinations were made by calibrating with $Fe(n,\gamma)$, $S(n,\gamma)$, and $H(n,\gamma)$. An Y^{88} source was also used.

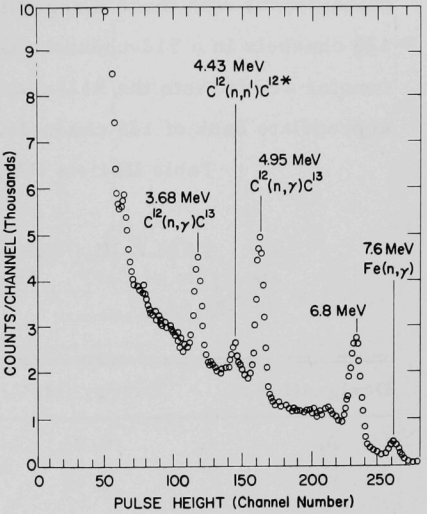

Fig. 15. Gamma rays from carbon target. Data collected in 16 hours.

The 2-D system was used to study coincidences of the gamma rays from Ca^{45}. This system is in effect a 4-channel analyzer in coincidence with 128 channels. The output of one counter is fed to a 100-channel analyzer. This analyzer can be divided into four windows of any width in the 100-channel range. Thus we can select 4 regions of the spectrum and search for

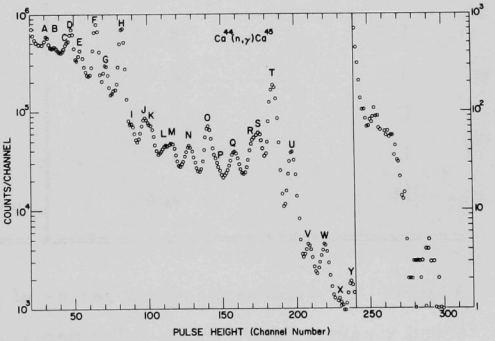

Fig. 16. Spectrum of capture gamma rays from Ca^{44}. The full energy range is about 8 MeV.

coincidences with these 4 regions. Each of these windows gates a bank of 128 channels in a 512-channel analyzer. The pulses from the second counter are fed into the 512-channel analyzer and are recorded in the appropriate bank of 128 channels.

Table III lists the gamma rays designated by letter.

TABLE III. Gamma rays observed in the singles spectrum of Ca^{45}. The letter designations correspond to Fig. 16.

Designation	Energy (MeV)	Designation	Energy (MeV)
A	0.84	N	3.43
B	0.95	O	4.04
C	1.14	P	4.26
D	1.26	Q	4.35
E	1.41	R	4.96
F	1.73	S	5.16
G	1.81	T	5.50
H	2.17	U	6.04
I(?)	2.41	V	6.48
J	2.63	W	6.85
K	2.86	X	7.27
L	3.12	Y	7.56
M	3.28		

Figures 17 — 22 represent a series of spectra in coincidence with selected γ rays. Much more coincidence work is required before a satisfactory analysis of the decay scheme can be made. A preliminary scheme is offered in Fig. 23. This is extremely fragmentary. As intensities are calculated and additional coincidences are studied, additional levels will be discovered.

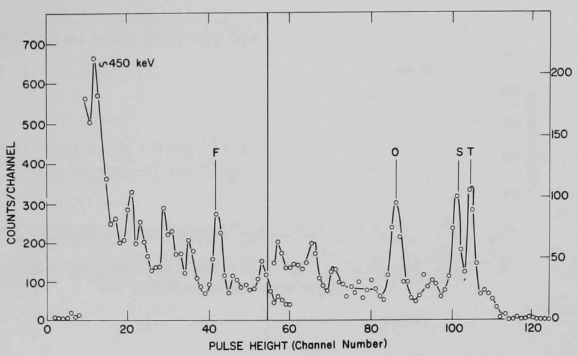

Fig. 17. Spectrum in coincidence with peak A of Fig. 16. The full energy range is about 8 MeV.

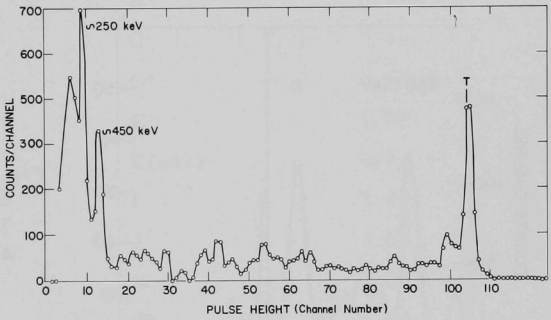

Fig. 18. Spectrum in coincidence with peak F of Fig. 16. The full energy range is about 8 MeV.

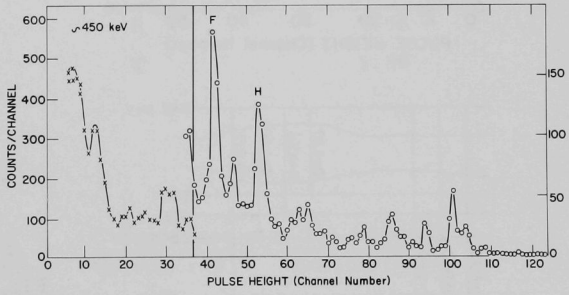

Fig. 19. Spectrum in coincidence with peak H of Fig. 16. The full energy range is about 8 MeV.

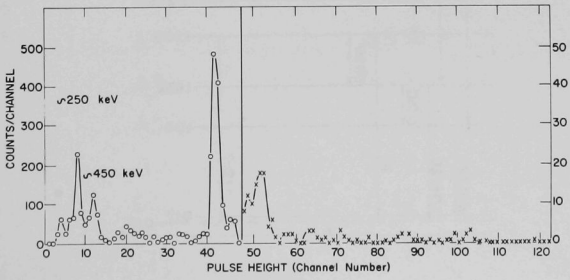

Fig. 20. Spectrum in coincidence with peak T of Fig. 16. The full energy range is about 8 MeV.

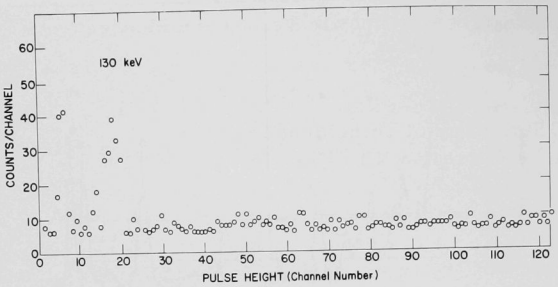

Fig. 21. Spectrum in coincidence with peak T of Fig. 16. The full energy range is 1 MeV.

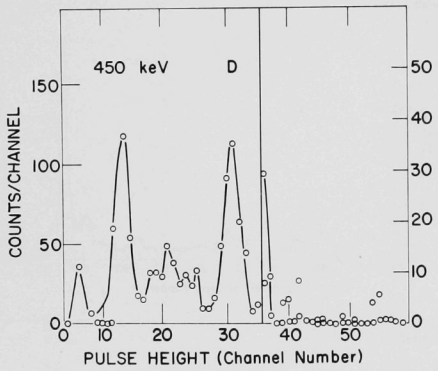

Fig. 22. Spectrum in coincidence with peak U of Fig. 16. The full energy range is about 8 MeV.

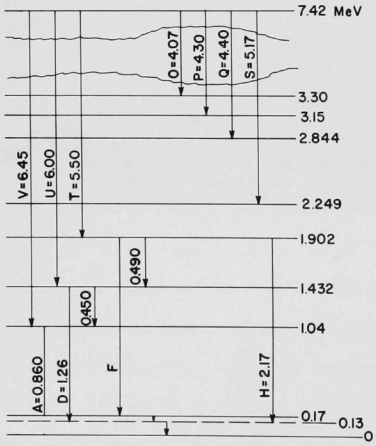

Fig. 23. Partial decay scheme of Ca^{45}. This is to be considered very preliminary.

Table IV summarizes our knowledge of coincidences as of this date.

TABLE IV. Summary of coincidence data.
The letter designations correspond to Fig. 16.

Coincidences with A(0.840 MeV)	
Gamma ray	Energy (MeV)
A'	0.450
A	0.840
C	1.14
D	1.26
D' (?)	1.30
E	1.41
F	1.73
G	1.81
I	2.41
K	2.86
L	3.12
O	4.04
Q	4.35
S	5.16
T	5.50

Coincidences with F(1.73 MeV)	
Gamma ray	Energy (MeV)
A"	0.250
A'	0.450
C	1.14
D'	1.30
E'	1.50
F(acc)	1.73
I	2.41
J	2.63
K	2.86
O	4.04
R	4.96
T	5.50

Coincidence with H(2.17 MeV)	
Gamma ray	Energy (MeV)
A'	0.450
A	0.840
B	0.950
C	1.14
D	1.26
E	1.41

Coincidence with T(5.50 MeV)	
Gamma ray	Energy (MeV)
A^{iv}	0.040
A'''	0.130
A"	0.25
A'	0.450
A	0.84
D'	1.30

TABLE IV. (cont'd)

Coincidence with H(2.17 MeV)	
Gamma ray	Energy (MeV)
F	1.73
G	1.81
H	2.17
I	2.41
K	2.86
L	3.12
M	3.28
M'	3.10
N	3.43
O	4.04
P	4.26
Q	4.35
S	5.11

Coincidence with T(5.50 MeV)	
Gamma ray	Energy (MeV)
E'	1.50
F	1.73
G	1.81

Coincidence with U(6.04 MeV)	
Gamma ray	Energy (MeV)
A'	0.45
A	0.840
D	1.26

I-57-1 Mu-Mesonic X Rays from Atoms with $7 \leq Z \leq 30$ (51210-01)

C. S. Johnson* and H. L. Anderson,*
E. P. Hincks,† S. Raboy, and C. C. Trail
Reported by S. Raboy and C. C. Trail

1. INTRODUCTION

When a muon comes to rest in a stopping material, a mesonic atom is formed and x rays are emitted as the muon cascades to the K shell of the atom. Because the muon mass is about 200 times the electron mass, the radii of the Bohr orbits are correspondingly

*University of Chicago

†National Research Council of Canada

smaller and the energy levels of the mesonic atoms are quite sensitive to the nuclear charge distribution. Wheeler[1] first suggested that a careful measurement of the energies of these mesonic x rays would give some information about the size of the nuclear charge.

Recent electron-scattering measurements yield a great deal of information about the nuclear charge distribution. Ford and Wills[2] have used the parameters obtained from these scattering experiments to calculate the energies of these transitions and it is interesting to compare the calculations with energies deduced from x-ray measurements.

Johnson, Hincks, and Anderson[3] recently reported some energies of K_α x rays but their measurements showed a systematic difference from the values calculated by Ford and Wills.[2] The differences were largest in the iron region of the periodic table.

In order to examine the differences more carefully, the scintillation spectrometer[4] with an anticoincidence annulus of NaI was used. This instrument and an associated computer program[5] permit one to obtain the full benefit of the statistical accuracy of the data.

X rays from N, O, F, Mg, Ca, Ti, Ni, Cu, and Zn have been observed. The data from Mg, Ti, Ni, Cu, and Zn have been analyzed and are reported here. The results from the other elements will be given in an early report. Data were also obtained with separated isotopes of Ca^{40} and Ca^{44} to observe any isotopic shift that might be present. These data have not been analyzed.

[1] J. A. Wheeler, Revs. Modern Phys. 21, 133 (1949).

[2] K. W. Ford and J. G. Wills, Nuclear Phys. 35, 295 (1962).

[3] C. S. Johnson and E. P. Hincks, and H. L. Anderson, Phys. Rev. 125, 2102 (1962).

[4] C. C. Trail and S. Raboy, Rev. Sci. Instr. 30, 425 (1959).

[5] R. Julke, J. E. Monahan, S. Raboy, and C. C. Trail, Argonne National Laboratory topical report ANL-6499 (unpublished).

2. EXPERIMENTAL ARRANGEMENT AND APPARATUS

The experiment was performed with the 150-MeV/c negative muon beam from the University of Chicago synchrocyclotron.

A sketch of the apparatus is shown in Fig. 24. In addition to negative muons, a large number of pions and electrons are in the beam.

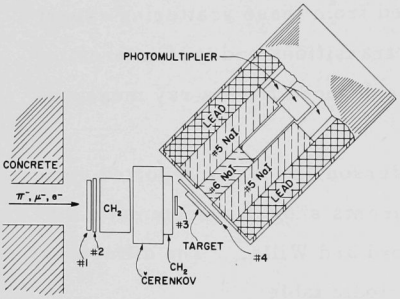

Fig. 24. Top view of the apparatus. Counters 1, 2, 3, and 4 are plastic scintillators. C is a water Čerenkov counter. Counter 6 is a NaI scintillation spectrometer and counter 5 is an anticoincidence annulus of NaI.

The beam passes through three scintillation counters (labeled 1, 2, and 3 in Fig. 24), a paraffin moderator, and a Čerenkov counter. The paraffin absorbs the π mesons and slows down the muons so that they stop in the target. The Čerenkov counter gives a pulse if the high-energy electron passes through it and in this way discriminates against these particles.

Counter 4 is used in anticoincidence to indicate that a meson has stopped in the target and no charged particle has entered the NaI spectrometer.

If a muon stops in the target, the emitted x rays may be detected with a NaI scintillation spectrometer. If the x-ray quantum loses all its energy in counter 6 (a cylinder of NaI 2.4 in. in diameter and 6 in. long) then the pulse is analyzed in a multichannel analyzer. If some of the energy is lost from counter 6 but is detected in a NaI annulus (counter 5), then the pulse is discarded electronically. The annulus is 12 in. long and 8 in. in diameter and has a hole 2.5 in. in diameter along its axis.

An event of interest, then, is denoted symbolically as (1, 2, 3, $\overline{4}$, $\overline{C}$, $\overline{5}$, 6). Figure 25 gives a block diagram of the electronics.

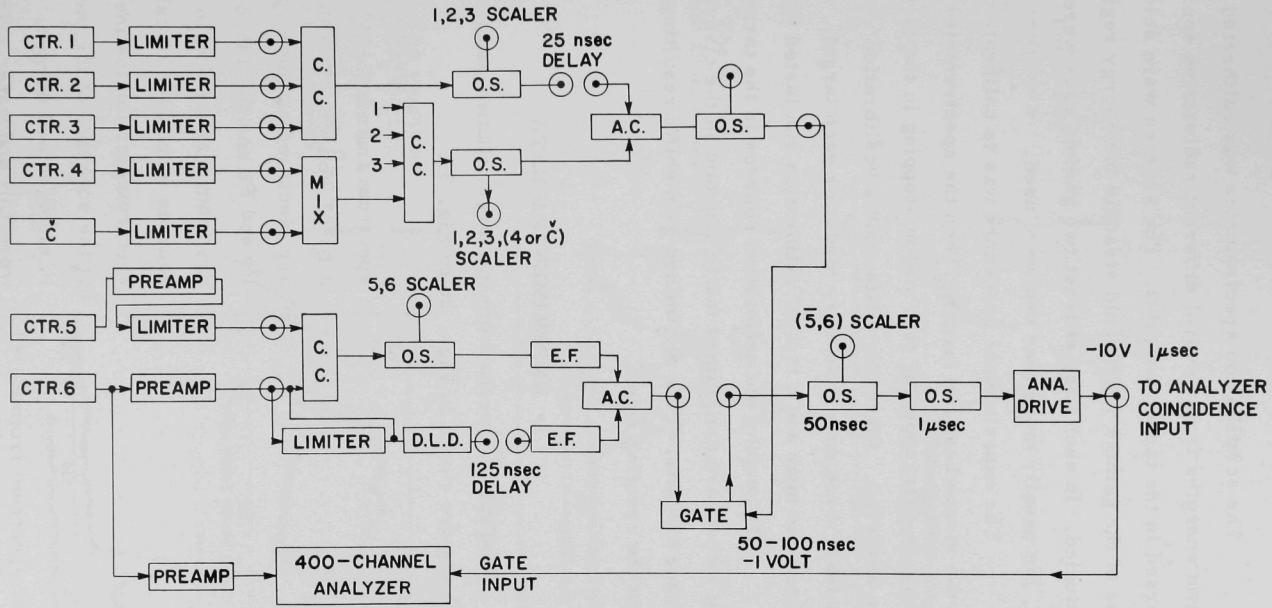

Fig. 25. Block diagram of the electronics. Abbreviations used in the figure are: O.S., one-shot univibrator; E.F., emitter follower; A.C., anticoincidence circuit; C, coincidence circuit; C̄, Čerenkov counter; D.L.D., delay-line drive; and ANAL. DRIVE, analyzer drive.

The scintillation spectrometer was calibrated with gamma rays of known energies from several different radioactive sources which were immersed in the target material. The sources were selected so that the energies of the gamma rays would straddle the energy region of the x ray being studied. In each case at least two gamma rays were used for calibration, but usually more than two were used.

The experimental procedure was to calibrate the spectrometer with the meson beam on target. Then the spectrometer was gated with those events corresponding to a meson stopping in the target and the x rays were observed. After this "data run" a "calibration run" was repeated. At least three data runs were made for each target. A typical data run lasted one hour and a typical calibration run lasted fifteen minutes.

By keeping the calibration sources in the target material, the counting rates were maintained fairly constant in the circuits before the coincidence circuits. This minimized gain shifts resulting from variations in the counting rates.

3. EXPERIMENTAL DATA

Typical spectra from the target studied and from the calibration runs are shown in Figs. 26 to Fig. 39.

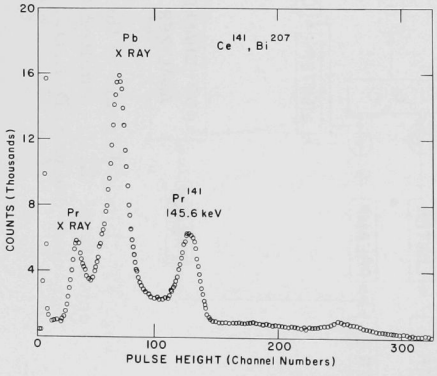

Fig. 26. The spectrum from Ce^{141} and Bi^{207}. This is a calibration run for the nitrogen and oxygen measurements.

Figure 26 shows a spectrum from a Ce^{141} source and a Bi^{207} source. The three peaks are identified as the x rays from Pr and Pb and the 145.6-keV gamma ray from a transition in Pr. These sources were used to calibrate the spectrometer for the measurements of the energies of the mesic x rays in nitrogen and oxygen. The targets were LiN and water. The spectra

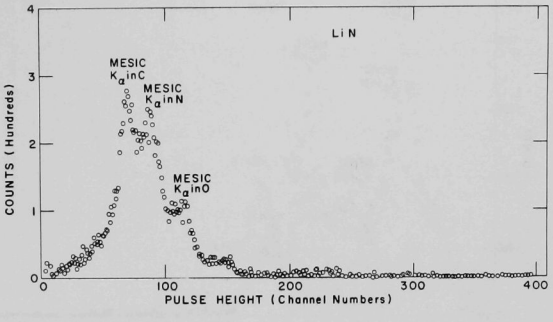

Fig. 27. The x-ray spectrum from a target of LiN.

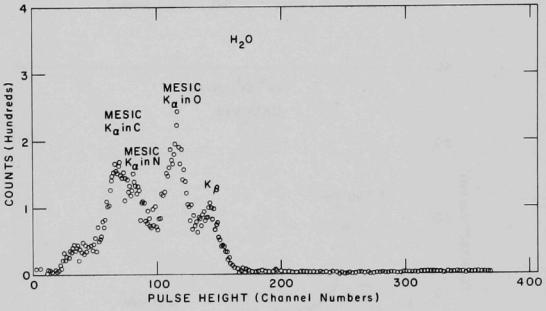

Fig. 28. The x-ray spectrum from a water target.

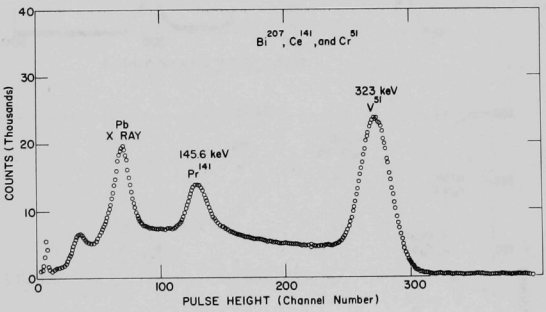

Fig. 29. The spectrum from Bi^{207}, Ce^{141}, and Cr^{51}. This is a calibration for the fluorine measurements.

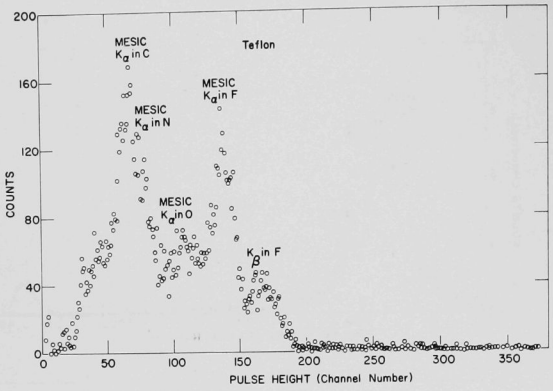

Fig. 30. The x-ray spectrum from a teflon target (CF_2).

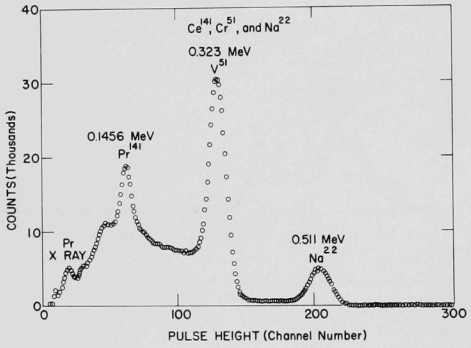

Fig. 31. A spectrum from Ce^{141}, Cr^{51}, and Na^{22}. This set of data is a calibration for the Mg x-ray measurements.

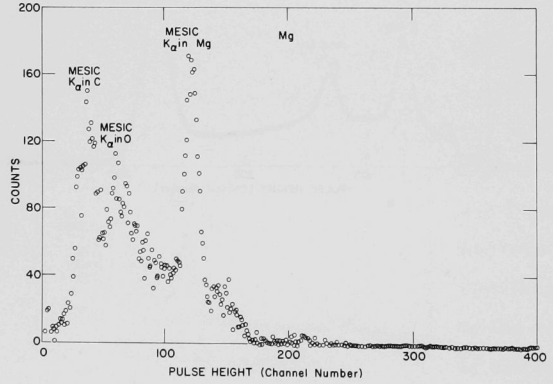

Fig. 32. The x-ray spectrum from a Mg target.

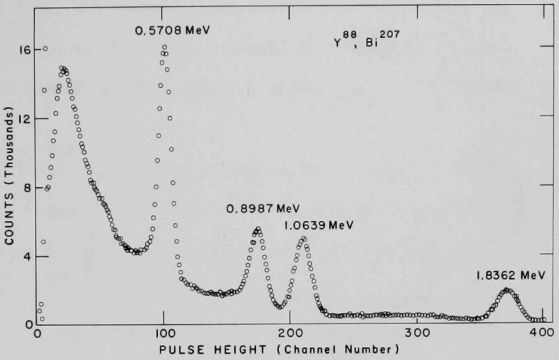

Fig. 33. A calibration spectrum with Y^{88} and Bi^{207} for the Ti x-ray measurements.

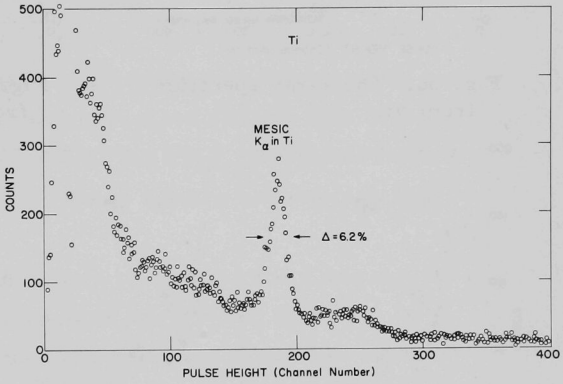

Fig. 34. The x-ray spectrum from titanium.

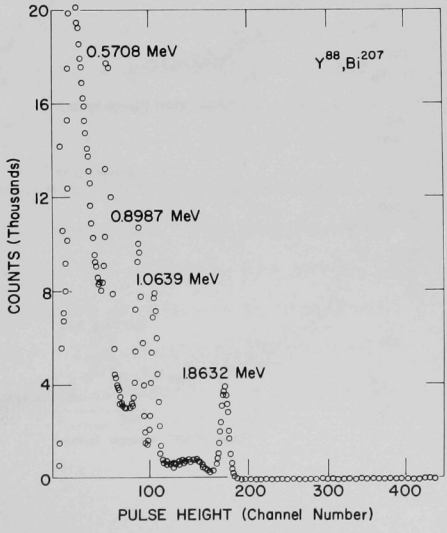

Fig. 35. A calibration spectrum from Y^{88} and Bi^{207}.

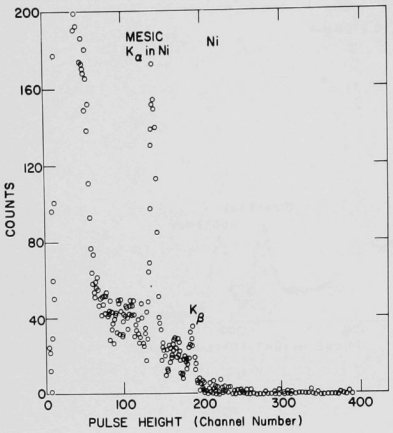

Fig. 36. The x-ray spectrum from Ni.

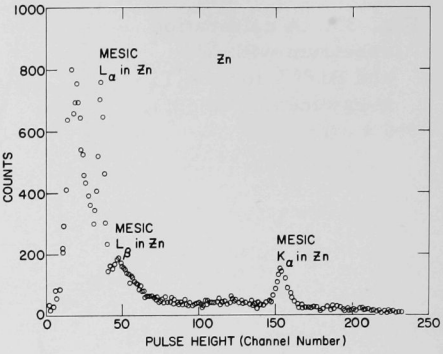

Fig. 37. The x-ray spectrum from Zn.

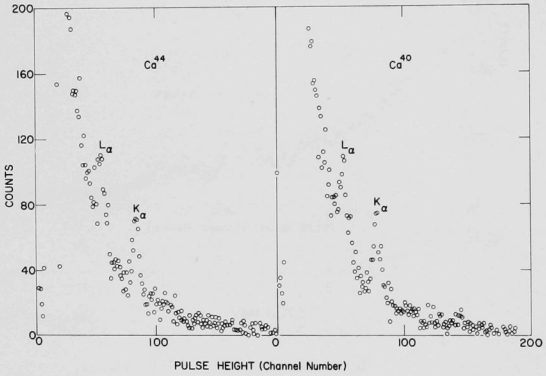

Fig. 38. The x-ray spectrum from Ca^{44} and Ca^{40}.

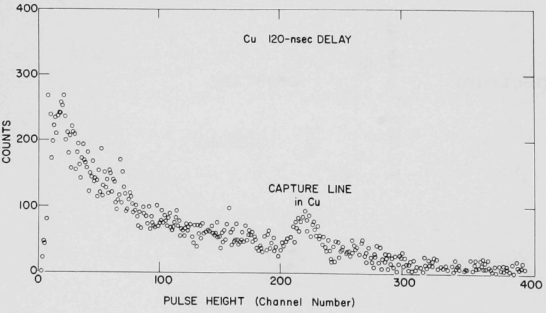

Fig. 39. The delayed gamma-ray spectrum from copper, showing a capture gamma ray.

from these targets are shown in Fig. 27 and 28. In addition to the lines of interest in these figures, there are also x rays which we attribute to carbon and oxygen in the various counters and their packaging and to the nitrogen in the air.

Figure 29 gives a calibration run made with the Bi^{207} and Ce^{141} sources shown in Fig. 26 and Cr^{51} which gives a 323-keV gamma ray. This calibration was used to measure the energy of the fluorine x rays. The spectrum from teflon (CF_2) is shown in Fig. 30.

Figures 31 and 32 show a calibration run and a data run for Mg. The calibration was made with the 140-keV gamma ray from Ce^{141}, the 323-keV gamma ray from Cr^{51}, and the 511-keV annihilation radiation from Na^{22}. Figure 32 gives the data run from Mg.

The spectrometer was calibrated with the 898.4- and 1836-keV lines from Y^{88} and the 570.8- and 1063.9-keV lines from Bi^{207} for the measurement on Ti. These spectra are shown in Figs. 33 and 34.

Figures 35 and 36 show a calibration and a data run for a nickel target. The calibration sources are Y^{88} and Bi^{207}.

Figure 37 gives the calibration and x-ray data from the zinc measurements. Again the calibration sources are Y^{88} and Bi^{207}.

It is interesting to note that in the x-ray spectra from the targets with higher Z, some other x-ray transitions are evident. In the spectra from nickel and zinc, the K_β, K_∞, and the L series of transitions are evident.

Figure 38 shows the x-ray spectrum from two isotopes of calcium. These data represent twelve 5-min runs. The targets were switched after each run and a separate bank of 200 channels was used to store the data from each target. The purpose of this was to measure an isotopic shift in the K_α transition energy. The amount of the shift is expected to be about 2 keV in 900 keV. The spectrometer was calibrated with Y^{88} and Bi^{207} sources.

4. RESULTS

The data from the calibration runs and data runs were analyzed in a manner described previously.[5] Briefly, each photopeak is fitted with a Gaussian function of the form

$$f(a,x_j) = a_1 e^{\frac{(x_j - a_2)^2}{a_3^2}} + a_4, \quad (1)$$

where $f(a,x_j)$ is the number of counts in channel x_j, a_1 is the amplitude of the Gaussian, a_2 its position, a_3 its width, and a_4 any constant background which may be present.

These fits are made on the ANL computer GEORGE and the best fit is determined by a chi-squared minimization calculation.

The normal procedure for the calibration runs is to fit the highest energy photopeak, subtract out its influence on a lower energy peak (by using a spectrum from each source alone), and then fit the next highest peak, etc.

The data runs are analyzed in a similar fashion, and the backgrounds are obtained from targets whose x rays are of much lower energies than those from the target being analyzed.

Table V gives a summary of these fits for a typical calibration run and for a fit to the data run. The table lists the parameters of the Gaussian, their associated uncertainties, and the calculated and expected values of χ^2. (The expected value of χ^2 is N - 4 - 1, where N is the number of points used in the fit and 4 is the number of parameters.) In each case, the uncertainties associated with the parameters have been adjusted for the differences between the expected and calculated values of χ^2.

It was assumed that a linear relationship of the form

$$E = a\, a_2 + b \quad (2)$$

TABLE V. The parametersof Eq. (1), determined by minimizing χ^2. These results are for a calibration run and for a data run for the copper measurements.

Energy of gamma ray (keV)	Peak height a_1 (counts)	Mean of Gaussian a_2 (channels)	Standard deviation a_3 (channels)	Residual background a_4 (counts)	χ^2	
					This calculation	Expected value
1836.2	5456 ± 58	177.134 ± 0.034	5.50 ± 0.08	315 ± 52	24	15
1063.9	14106 ± 67	103.322 ± 0.011	4.18 ± 0.03	630 ± 60	6	11
898.7	13600 ± 144	87.399 ± 0.020	3.86 ± 0.06	957 ± 145	13	9
570.8	44631 ± 358	55.858 ± 0.015	3.07 ± 0.03	2289 ± 268	29	7
Cu K_α	97 ± 7	147.52 ± 0.21	4.50 ± 0.46	22 ± 6	11	12

describes the spectrometer's response to gamma rays. In Eq. (2), E is the energy of a gamma ray, a_2 is its mean pulse height determined from Eq. (1), and a and b are parameters to be determined. The peak positions from a calibration run are used to make a least-squares fit to Eq. (2). Again a value of χ^2 is computed and compared with the expected value. The uncertainties associated with the parameters a and b are adjusted accordingly.

Table VI lists a typical fit to Eq. (2).

TABLE VI. The parameters of the relation $E = a + ba_2$ for the calibration run for copper shown in Table VII.

Standard γ-ray energy E (keV)	Mean position of peak, a_2	Parameters of calibration relation		
		a (keV)	b (keV/channel)	χ^2
1836.2 ± 1.7	177.134 ± 0.034			
1063.9 ± 0.3	103.322 ± 0.011	- 11.34 ± 1.69	+ 10.410 ± 0.17	5
898.7 ± 0.8	87.399 ± 0.020			
570.8 ± 0.5	55.858 ± 0.015			

Some of the K_a energies have been determined and are listed in Table VII. The errors are a combination of random and

TABLE VII. Summary of results.

Target x-ray	Energy (keV)
Mg K_a	300.2 ± 0.6
Ti K_a	939.0 ± 1.5
Ni K_a	1436.9 ± 2.1
Cu K_a	1525.2 ± 5.4
Zn K_a	1607.9 ± 1.3

systematic errors. It must be emphasized that these results are preliminary. When all the calculations are compiled, final results will be presented along with a comparison with other measurements and theoretical calculations. In general our results seem higher than theory predicts.[2]

Finally, a study was made to see if any gamma rays are emitted as the muon is captured by the nucleus and the energy is released by some form of nuclear breakup. This process is studied by observing those gamma rays emitted 120 nsec after the muon comes to rest in the target. We show this spectrum from copper in Fig. 39. Of the nuclei studied, only this one exhibited these capture gamma rays. The peak near channel 200 is tentatively identified as a gamma ray in Ni^{62} at 1.1 MeV.

II. MASS SPECTROSCOPY

II-26-1 Ionization by Ions in the MeV Range (51300-01)

S. Wexler and D. C. Hess
Reported by S. Wexler

A. INTRODUCTION

Investigation of the properties of the interactions (e.g., charge exchange and ionization) of massive ionic projectiles with gases has mainly been confined to energies in the range below 200 keV.[1] Most of the studies with projectiles of kilovolt energy have involved measurement of cross sections for various reactions. But a Russian group[2] has employed a mass spectrometer to analyze the charge distributions of slow interaction products. Only three determinations of a molecular fragmentation pattern, all for H_2, by impact of protons and hydrogen atoms with energies of 10 — 180 keV have been reported.[3] Measurements of the cross sections for ionization of several gases by protons and He^+ have been published for impinging particles with energies up to 1.1 MeV.[4] But there have been no mass spectrometric

---

[1] See the review of J. B. Hasted, Advances in Electronics and Electron Physics 13, 31 (1960).

[2] N. V. Fedorenko, V. V. Afrosimov, R. N. Ilín, and E. S. Solov'ev, Proceedings of the 4th International Conference on Ionization Phenomena in Gases, edited by N. R. Nilsson (North-Holland Publishing Co., Amsterdam, 1960), Vol. I, p. 47.

[3] N. V. Fedorenko, R. N. Ilín, and E. S. Solov'ev, Proceedings of the 5th International Conference on Ionization Phenomena in Gases, edited by H. Maecker, (North-Holland Publishing Co., Amsterdam, 1962), Vol. II, p. 1300; J. P. Keene, Phil. Mag. 40, 369 (1949); V. V. Afrosimov, R. N. Ilín, and N. V. Fedorenko, JETP 34, 968 (1958).

[4] J. W. Hooper, E. W. McDaniel, D. W. Martin, and D. S. Harmer, Phys. Rev. 121, 1123 (1961); ibid. 125, 2000 (1962); R. A. Langley, Annual Summary Report No. 10, March 1, 1962 (Georgia Institute of Technology Engineering Experiment Station, Atlanta).

analyses of the slow ions resulting from impact of a beam of MeV ions with isolated atoms and molecules.[5]

Apart from the fact that the results would in themselves be of fundamental interest, there are other reasons for entering the virtually untouched field in which massive projectile ions with energies in the MeV region interact with isolated molecules. Firstly, in controlled thermonuclear devices, the nuclear reactions D(d, n)He^3 and D(d, p)T followed by D(t, n)He^4 and D(He^3, p)He^4 may be utilized. The protons, tritons, and singly-charged He^3 are produced in these reactions with kinetic energies of up to a few MeV. Consequently, particularly in pulsed machines, their extranuclear interactions with D_2 and impurity gases in incompletely ionized plasmas may be of interest in understanding the behavior of these plasmas.[6] Again, such studies have a direct bearing on the effects of atomic and molecular structure on the stopping power of gases and other aspects of penetration phenomena.[7] A specific example is the details of energy transfer and molecular disruption in the slowing down of energetic recoils from nuclear reactions, e.g., tritium from

---

[5] C. E. Melton and P. S. Rudolph [J. Chem. Phys. 30, 847 (1959)] have ionized acetylene with the radiation of a Po^{208} alpha source in the source chamber of a mass spectrometer.

[6] R. F. Post, Revs. Modern Phys. 28, 338 (1956); K. Bockasten, R. Hallin, S. I. Herlitz, L. Högberg, N. R. Nilsson, S. Svennerstedt, and K. Vogel, "Controlled Thermonuclear Fusion Research," International Atomic Energy Agency Review Series, No. 17 (1961). See also the extensive bibliography on plasmas and other work related to controlled thermonuclear research in "Atomic and Molecular Collision Cross Sections of Interest in Controlled Thermonuclear Research," ORNL-3113 (May 15, 1961).

[7] R. L. Platzman, Int. J. Appl. Radiation and Isotopes 10, 116 (1961); H. A. Bethe and J. Ashkin, Experimental Nuclear Physics, edited by E. Segré, (John Wiley and Sons, Inc., New York, 1953) Vol. 1, p. 166.

$He^3(n,p)T$.[8] Also, experiments in this range of projectile energies make possible a test of a consequence of the Born approximation, namely, that the fragmentation pattern when a molecule is ionized and excited by a massive ion is the same as for electron impact if the velocities are the same and are sufficiently high.[9] Melton and Rudolph[5] have reported that C_2H_2, irradiated by a Po^{208} alpha source placed in the source chamber of their mass spectrometer, breaks down into a very simple ionic mass pattern. Only the parent $C_2H_2^+$ (relative abundance = 100) and the fragment ion C_2H^+ (R.A. = 7.7) were observed. This is an unexpected result because the fragmentation pattern of acetylene bombarded by electrons of the same velocity as the α particles is much more extensive and is not much different from that arising from impingement of 70-eV electrons.[10] Consequently, it is considered of interest to study the fragmentation of C_2H_2 (as well as other molecules) by impingement of massive particles with energies in the MeV range. Finally, the interactions of helium ions and protons with rarefied air has a bearing on understanding the origin of the aurora borealis and other upper-atmospheric phenomena.[11]

As the initial study of a program to investigate the ionization of isolated molecules by swiftly-moving ions with energies in the range from a few hundred keV to a few MeV, we have bombarded several of the rare gases and lower hydrocarbons with protons coming from the

---

[8] R. J. Cross, Jr. and R. Wolfgang, J. Chem. Phys. 35, 2002 (1961); P. J. Estrup and R. Wolfgang, J. Am. Chem. Soc. 82, 2665 (1960).

[9] H. Bethe, Ann. Phys. 5, 325 (1930); N. F. Mott and H. S. W. Massey, The Theory of Atomic Collisions (Oxford University Press, London, 1949), pp. 247, 271; P. Kebarle and E. W. Godbole, J. Chem. Phys. 36, 302 (1962).

[10] H. E. Stanton and J. E. Monahan, J. Chem. Phys. 37, 2654 (1962); P. Kebarle and E. W. Godbole, ibid. 36, (1962); C. E. Melton, ibid. 37, 562 (1962).

[11] A. B. Meinel, Astrophys. J. 113, 50 (1951); C. V. Fan and A. B. Meinel, ibid. 118, 205 (1953).

Van de Graaff electrostatic generator with energies of 0.80 — 3.75 MeV. A specially-designed portable mass spectrometer was constructed on a frame provided with casters and jacks so that it can readily be moved into position and aligned with the beam of high-energy ions. The source section of the apparatus is sketched in Fig. 40. The energy-analyzed beam

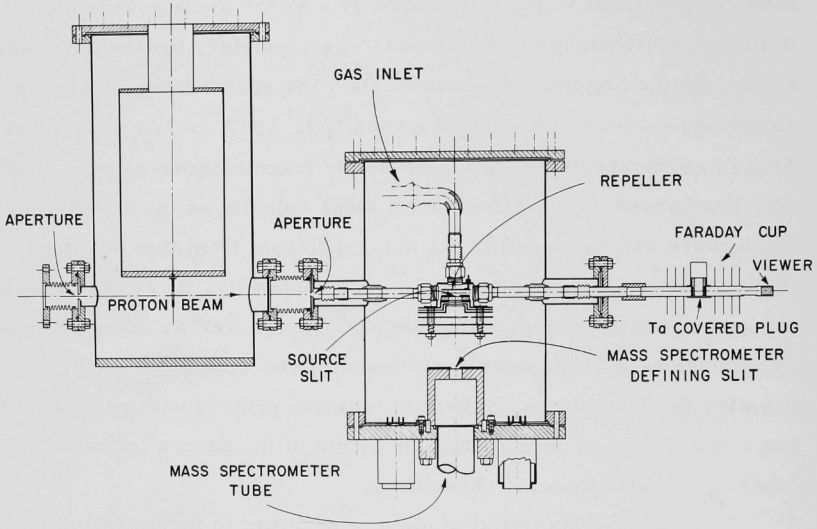

Fig. 40. Source assembly of the mass spectrometer for study of impact phenomena of protons and molecules with energies in the MeV range.

of protons is collimated by two slits 1.25 mm square and passes through two apertures $\frac{3}{16}$ in. in diam. and a large aperture in a cold diaphragm at liquid N_2 temperature before passing through the target gas on a path midway between the repeller plate and the exit slit of the source chamber. The beam finally is monitored in a deep Faraday cup, in which it is stopped by a tantalum-coated plug. The slow positive ions are extracted at 90° to the direction of the proton beam, focused and accelerated by a Nier-type focusing system, analyzed by a 90°-sector magnetic field of 9-in.

radius, and detected by a plate surrounded by guard rings and an electron-suppressor electrode. The proton beam was about 3.0 μA; and the current of slow ions, measured with a vibrating-reed electrometer, varied between 5×10^{-14} and 1×10^{-10} amp. The source chamber and focusing system were held at or near 5500 V relative to the grounded spectrometer tube. The gas pressure in the source was $3-6 \times 10^{-4}$ mm which, as attested by the linear pressure dependence of the intensities of the charge states of Ne (Fig. 41), is sufficiently low to ensure that a proton will interact only once with the gas. Differential pumping reduced the pressures in the other compartments of the spectrometer to less than 5×10^{-6} mm.

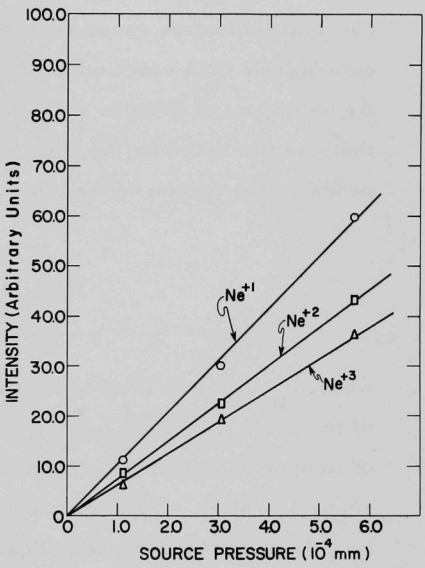

Fig. 41. Intensities of ionic species as a function of the pressure of Ne in the source chamber of the mass spectrometer.

A careful measurement of the secondary-electron currents to the repeller plate and to the source chamber showed that the respective ratios of secondary electrons to primary protons were 0.00040 and 0.00055 under the conditions of the experiment.

B. RESULTS

The slow product species from impact of protons with the rare gases consist of ions in various charge states. From each intensity distribution one may determine the partial cross section for production of each charge state provided the total ionization cross section for the rare gas is known. This determination is based on the fact

that, as may readily be shown, the total and partial cross sections are related by

$$\sigma_n = \frac{I_n}{\sum I_n} \frac{1}{n} \sigma_{total}, \tag{1}$$

where σ_n is the cross section for formation of the ionic species of charge state +n, $I_n / \sum I_n$ is the fractional intensity of the species, and σ_{total} is the total ionization cross section for the target gas. Hooper et al.[4] have determined such reaction probabilities for the ionization of He, Ne, and Ar by impact of protons with energies of 0.15 — 1.1 MeV. They find that, as predicted by the Born approximation, the total cross section depends on the proton energy through the relation

$$\sigma_{total} = \frac{A}{E_p} \log BE_p, \tag{2}$$

where σ_{total} is the total ionization cross section, A and B are constants of the particular atom, and E_p the proton energy. Both the data of Hooper and theoretical arguments[9,12] indicate that Eq. (2) is valid above 1.1 MeV. We have used our data on n and fractional intensities $I_n / \sum I_n$ in combination with Eqs. (1) and (2) to compute the partial cross section for formation of each charge state of several of the rare gases. They are plotted in Figs. 42 through 44. Included in each figure are curves representing the data of Fedorenko et al.[13] for the

[12] D. R. Bates and G. Griffing, Proc. Phys. Soc. (London) A66, 961 (1953); R. A. Mapleton, Phys. Rev. 109, 1166 (1958).

[13] N. V. Fedorenko, V. V. Afrosimov, R. N. Ilin, and E. S. Solov'ev, Proceedings of the 4th International Conference on Ionization Phenomena in Gases, edited by N. R. Nilsson (North-Holland Publishing Co., Amsterdam, 1960), Vol. I, p. 47.

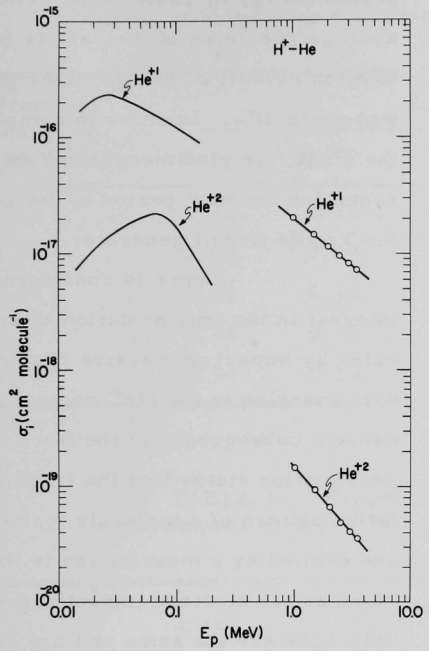

Fig. 42. Ionization cross sections for formation of He^{+1} and He^{+2} by proton impact. The data points represent the results of this study in the energy region from 1.00 to 3.50 MeV. The curves in the range from 5 to 180 keV are taken from Fedorenko et al. (reference 13).

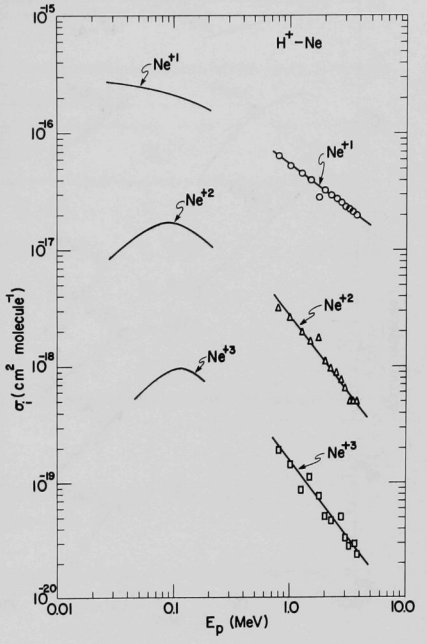

Fig. 43. Ionization cross sections for formation of Ne^{+1}, Ne^{+2}, and Ne^{+3}.

range of proton energies extending from 5 to 180 keV. Although a large gap still remains to be explored between the two sets of data, the results are reasonably concordant. The treatment of the data described above could not be extended to krypton because its total ionization cross sections have not been measured in this energy region. Accordingly, the fractional intensity of each charge state observed for Kr is tabulated as a function of

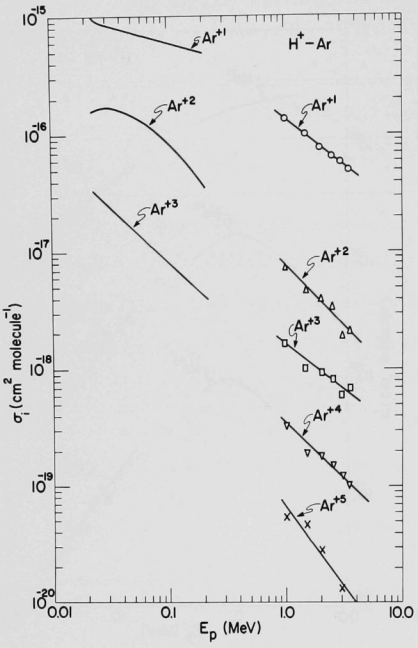

Fig. 44. Cross sections for production of Ar^{+1}, Ar^{+2}, Ar^{+3}, Ar^{+4}, and Ar^{+5} by proton impact on argon.

proton energy in Table VIII. The average precision of the results for krypton as well as for the other gases was about 10%. In order to complete the study, we plan measurements on xenon for our next period of use of the Van de Graaff generator.

There is considerable interest in the fragmentation of molecules by impact of massive projectiles with energies in the MeV region, because a consequence of the Born approximation states that the fragmentation pattern of a molecule ionized and excited by a massive ion is the same as for electron impact if the velocities are the same and are sufficiently high.[9, 12] As a beginning of an experiment to test the validity of this deduction from the Born approximation, we have bombarded several molecules with 2.25-MeV protons. As an example, the fragmentation spectrum observed for acetylene appears in Table IX. This pattern as well as those for the other molecules will be compared with corresponding ones found on electron impact under similar experimental conditions.

TABLE VIII. Fractional intensities of charge states of krypton as a function of proton energy.

Proton energy (MeV)	Charge state				
	Kr^{+1}	Kr^{+2}	Kr^{+3}	Kr^{+4}	Kr^{+5}
1.50	0.73	0.13	0.10	0.032	0.011
2.00	0.63	0.15	0.16	0.048	0.015
2.50	0.69	0.14	0.12	0.036	0.012
3.00	0.74	0.12	0.10	0.028	0.009
3.50	0.74	0.13	0.09	0.028	0.010

TABLE IX. Fragmentation pattern of C_2H_2 under impact by 2.25-MeV protons.

m/e	Relative intensity
26	100
25	30 ± 3
24	6.9 ± 0.5
13	4.7 ± 0.4
12	2.6 ± 0.2

II-40-11 Fragmentation of Hydrocarbons (51300-01)

H. E. Stanton and J. E. Monahan

AN ANALYSIS OF THE ENERGY DISTRIBUTION OF IONIC FRAGMENTS

Recent measurements[1] of the mass spectra resulting from high-energy electron impact on some hydrocarbon molecules are consistent with the assumption that some of the different types of ionic fragments are produced by the independent decay of the parent ion through at least two groups of noninteracting electronic states. The associated energy and the mechanism of the decay of each group of such states is expected to be different from the others. A quantitative measurement of the energy distribution of the ionic fragments may provide a definitive test of these assumptions.

Previous analyses[2] of measured energy distributions have not been satisfactory because of the cumbersome numerical calculations which were necessary in order to correct for the effects of finite slit widths, electron-beam divergence, and the inhomogeneous electric field in the ion chamber of the measuring apparatus. This note describes a method of analysis which is considerably simpler and potentially more accurate than that used previously.

Figure 45 is a sketch of the chamber where ions are formed in the mass spectrometer MA-17. The dotted lines indicate equipotential lines of an electric field of the type existing within the ion source. This field is necessary in order to focus an ion beam of usable intensity out of the chamber and through the energy analyzer.

---

[1] J. E. Monahan and H. E. Stanton, J. Chem. Phys. 37, 2654 (1962).

[2] H. E. Stanton and J. E. Monahan, Physics Division Summary Report, ANL-6326 (March 1961), p. 55.

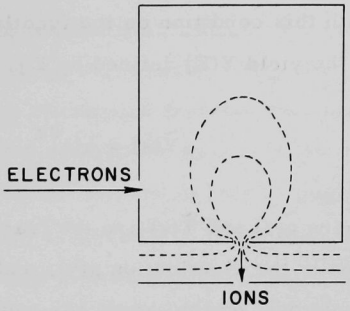

Fig. 45. A sketch of the ion chamber, showing the direction of incidence of the electron beam and the direction of emergence of the ion beam. The dotted lines indicate equipotential lines of a typical drawing-out field.

However, the drawing-out field causes some defocusing of the incident electron beam and, since ions are formed at different potentials, the measured distribution of the energy of formation is distorted by these spatial effects.

In the experimental arrangement described above, the measured yield Y(E) of a particular ionic fragment as a function of its kinetic energy is given by the equation

$$Y(E) = A \int_{E-b}^{E+b} d\epsilon \int_{0}^{\epsilon} dy\, g(y)\, T(\epsilon - y), \qquad (1)$$

where g(y) dy is the probability that the ion is formed in the region in which the electric potential is between y and y+dy, T(z)dz is the probability that at the instant of formation the ion has kinetic energy between z and z+dz, 2b is the energy equivalent of the slit widths of the energy analyzer, and A is the integrated intensity of the ion that is being analyzed.

The energy E is equal to the measured kinetic energy of the fragment if the potential y is assigned the value zero at the entrance slits of the energy analyzer. For this choice of zero potential, no ions are formed in the spatial volume associated with small values of y. In particular, no ions are formed for values of y less than the energy equivalent of the slit openings of the analyzer so that

$$g(y) = 0 \qquad \text{for} \qquad y \leq b. \qquad (2)$$

With this condition on the function g(y), the Laplace transform $\tilde{Y}(s)$ of the yield Y(E) defined by Eq. (1) becomes

$$s\tilde{Y}(s) = A(e^{sb} - e^{-sb})\,\tilde{g}(s)\,\tilde{T}(s), \tag{3}$$

where $\tilde{g}(s)$ and $\tilde{T}(s)$ are the transforms of g(y) and T(z), respectively. Ideally the distribution g(y), and consequently its transform $\tilde{g}(s)$, depends only on the target gas and the drawing-out field and not on the particular ionic fragment observed. Thus if $\tilde{Y}_p(s)$ denotes the transform of the yield of some standard fragment for which the corresponding distribution $\tilde{T}_p(s)$ is known, then from Eq. (3) the ratio of the transform of the yield of the measured fragment to that of the standard can be solved to give

$$\tilde{T}(s) = A_p\,\tilde{Y}(s)\,\tilde{T}_p(s)/\,[A\,\tilde{Y}_p(s)]. \tag{4}$$

All references to distortions caused by finite slit widths, inhomogeneous electric fields, and other perturbations have been eliminated by taking the ratio leading to Eq. (4) and the inverse transform of this equation represents the formal solution for the distribution of formation energy for the given ionic fragment.

If the yield distribution of the parent ion is taken as the standard, there is no kinetic energy due to fragmentation and the energy distribution is simply that of the thermal motion of the molecules of the target gas at the "temperature" Θ of the ion source, i.e.,

$$T_p(z) = 2z^{1/2}\, e^{-z/\Theta} \Big/ \sqrt{\pi\Theta^3}\,, \tag{5}$$

and

$$\tilde{T}_p(s) = (\Theta s + 1)^{-3/2}. \tag{6}$$

In order to avoid the numerical evaluation of the contour integral that gives T(z) in terms of the right-hand side of Eq. (4), the transform $\tilde{T}(s)$ can be obtained for any reasonable function T(z) and the parameters of the distribution evaluated directly by means of Eq. (4). For example, for fragmentation processes that result from a quasi-thermal excitation of the molecular ion (as postulated in the statistical theory of mass spectra[3]) it seems reasonable to assume that the distribution of fragmentation energy can be approximated by the Maxwell energy distribution for particles evaporated from a surface at "temperature" β. The distribution T(z) is obtained by "adding" the fragmentation energy and the energy associated with the thermal motion of the target gas, i.e.,

$$T(z) = \frac{2}{\beta^2\sqrt{\pi\Theta^3}} \int_0^z dx\, x^{1/2}\,(z-x)\exp\left[-\frac{x}{\Theta} - \frac{(z-x)}{\beta}\right]. \tag{7}$$

The transform of this distribution is

$$\tilde{T}(s) = (\Theta s + 1)^{-3/2}\,(\beta s + 1)^{-2}. \tag{8}$$

Substitution of Eqs. (8) and (6) into Eq. (4) gives

$$\frac{A}{A_p(\beta s + 1)^2} = \frac{\tilde{Y}(s)}{\tilde{Y}_p(s)}. \tag{9}$$

Thus the "measured" ratio $\tilde{Y}(s)/\tilde{Y}_p(s)$ has a second-order pole at $s = \beta^{-1}$ and the "temperature" β which completely characterizes the

---

[3] H. M. Rosenstock, M. B. Wallenstein, A. L. Wahrhaftig, and H. Eyring, Proc. Natl. Acad. Sci. US 38, 667 (1952).

distribution (7) can be determined directly from Eq. (9).

A second distribution which is of considerable interest is that which would apply if the fragmentation process starts from a repulsive electronic state in the parent molecular ion. In this case the distribution of the fragmentation energies becomes[2]

$$T(z) = C\, e^{-\alpha z} \sinh(\zeta \sqrt{z}), \tag{10}$$

where

$$C = \exp[-m'Q/(M\textcircled{H})] \Big/ \sqrt{\pi m' m \textcircled{H} Q / M^2}$$

$$\alpha = M/(m\textcircled{H}),$$

and

$$\zeta = 2\sqrt{Mm'Q/m^2\textcircled{H}^2}\,.$$

Here Q is the energy released in a fragmentation process in which a parent ion of mass M decays into a fragment ion of mass m and a neutral fragment of mass m'. The tranform of the distribution (10) is

$$\tilde{T}(s) = \sqrt{\pi}\; C(s+\alpha)^{-3/2} \exp[\tfrac{1}{4}\zeta^2 (s+\alpha)^{-1}], \tag{11}$$

and the value of Q that characterizes this distribution can be obtained from Eq. (4) which here takes the form

$$2\,\frac{A}{A_p}\left(\frac{M\textcircled{H}s + M}{m\textcircled{H}s + M}\right)^{3/2} \exp\left[-\left(\frac{m'sQ}{m\textcircled{H}s + M}\right)\right] = \frac{\tilde{Y}(s)}{\tilde{Y}_p(s)}\,. \tag{12}$$

The critical calculation in this analysis is the accurate evaluation of the ratio $\tilde{Y}(s)/\tilde{Y}_p(s)$ for a range of values of s sufficient for the determination of the parameters that characterize the distribution

function T(z). Since this ratio is defined in terms of measured quantities $Y(\epsilon)$ and $Y_p(\epsilon)$, i.e.,

$$\frac{\tilde{Y}(s)}{\tilde{Y}_p(s)} = \frac{\int_0^\infty d\epsilon\ e^{-s\epsilon}\ Y(\epsilon)}{\int_0^\infty d\epsilon\ e^{-s\epsilon}\ Y_p(\epsilon)}\ , \tag{13}$$

these transforms must be evaluated by numerical integration. This implies that the transforms must be approximated by integrals with finite upper limits. For $s \geq 0$ the error introduced by this approximation is of the order $(c + 1)e^{-c}$ where c is the ratio of the upper limit of the approximation integrals to the "temperature" of the fragment ion being considered. It is usually possible to measure the yield $Y(\epsilon)$ for values of ϵ such that $c \geq 5$.

A second point concerning the "measurement" of the ratio (13) should be mentioned. It is necessary that the yields $Y(\epsilon)$ and $Y_p(\epsilon)$ be measured relative to the same zero value for ϵ. If in the time inteval between the measurement of these yields the energy analyzer has drifted by an amount $\delta\epsilon$, then the calculated value of $\tilde{Y}(s)/\tilde{Y}_p(s)$ is $e^{s\,\delta\epsilon}$ times the true value. Such drifts must be taken into account analytically in order to obtain reliable values for the parameters of the distribution T(z) from this method of analysis.

V. THEORETICAL PHYSICS, GENERAL

V-1-2. Deformation Energy of a Charged Liquid Drop (51210-01)

S. Cohen and W. J. Swiatecki*
Reported by S. Cohen

The uniformly charged liquid drop has been used as a model for the calculation of many of the properties of nuclei. The application of this model to the process of nuclear fission has led to some understanding of qualitative features of the process but quantitative calculations have not been carried out for parameters corresponding to those of real nuclei. In the present study, results have been obtained which bear directly on the experimentally observed fission of nuclei. The results presented here were obtained by numerical techniques making use of an IBM-7090 computer.

For our model we consider a liquid drop with an electric charge distributed uniformly throughout its volume. In this idealization the total potential energy of the drop consists of two parts, the electrostatic energy E_c and the surface energy E_s due to the surface tension of the liquid. A dimensionless parameter, the fissionability parameter x, is used to characterize a given drop. This parameter can be considered as a measure of the charge on the drop. The parameter x for a drop of any shape is defined as equal to the quotient $(E_C/2E_S)_{sphere}$ for a spherical liquid drop with the same charge, volume, and surface tension as the drop under consideration. Nuclei which fission have values of x which range between 0.6 and 0.8.

We have restricted our calculations to shapes which are axially symmetric. The saddle-point shapes are further restricted to symmetry about a plane perpendicular to this axis; but small asymmetric distortions about this plane were considered in the investigations of the stabilities of the saddle-point shapes.

---

*Lawrence Radiation Laboratory, University of California, Berkeley.

In order to understand the significance of the saddle point in the potential-energy surface, it is perhaps best to consider the basic quantitative aspects of the problem. The sphere is always a shape of equilibrium for a charged liquid drop. For x less than 1.0 the sphere is a stable shape of equilibrium. For x larger than 1.0 it is an unstable shape of equilibrium.

As a gross approximation to the shape at the time of scission, i.e., at the instant of breaking apart in the fission process, let us consider two equal spheres in contact, the total volume and charge of these spheres being equal to the volume and charge of the original sphere. For $x > 0.34$ this configuration has a lower total energy than that of the single sphere. For $0.34 < x < 1.0$, therefore, the process is exothermic but not spontaneous since the spherical shape is itself stable. The particular value $x = 0.34$ is of course not the correct value since the simple configuration given is not one which is likely to occur in the fission process. The actual shape at scission depends on the dynamics of the problem and would be quite difficult to ascertain. Nevertheless for some value of x in this neighborhood the fission process does become exothermic. The excitation energy required for fission of the sphere is a problem of interest in this study.

In the configuration space describing the shapes of drops, consider now all possible paths that lead from one sphere to the unknown scission shape. The potential energy along this path must first rise (since the sphere is stable) but must eventually end up at a value below the initial value (since the process is exothermic). Consider now the maximum potential energy reached on this path. Every path must have such a maximum but the value depends upon the particular path followed. For some paths this maximum value is the smallest possible value. This least maximum is the least kinetic energy that the initial system must have in order to pass the potential barrier around the stable spherical shape. The configuration-space point corresponding to this least maximum is a saddle point in the potential-energy surface. If this saddle point is a maximum in

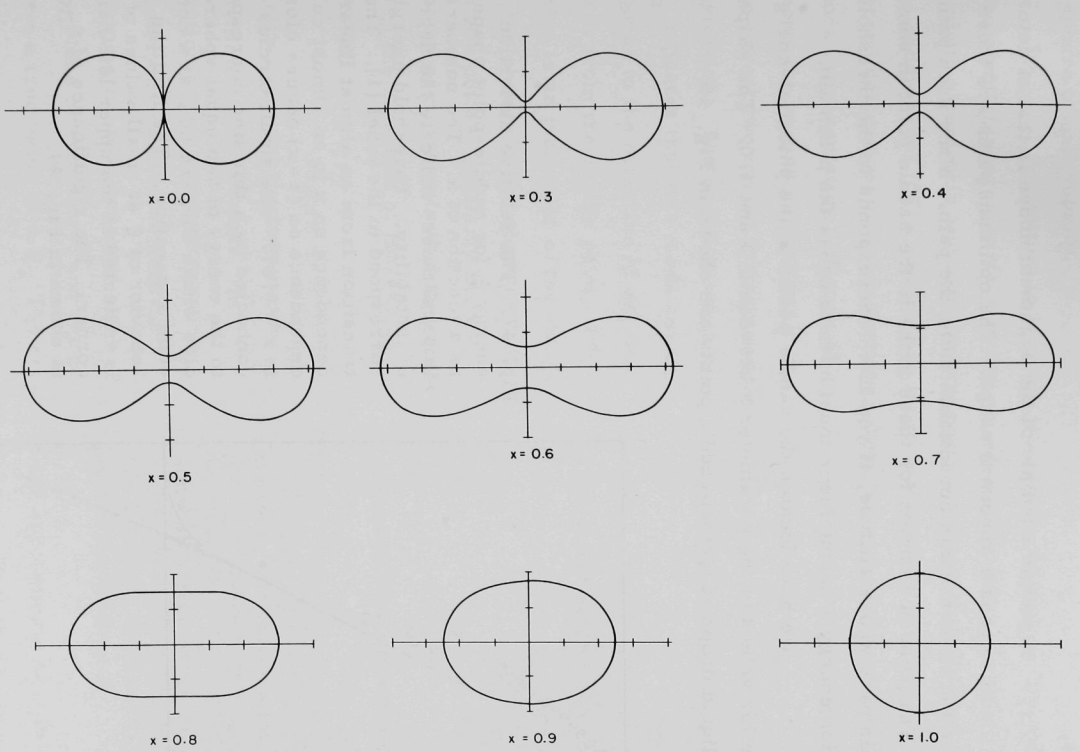

Fig. 46. Saddle-point shapes for various values of x.

only one direction, the value of the potential energy (relative to the sphere) at this point corresponds to the threshold energy for the fission process.

A simple example of the argument above is that of determining a path across a mountain range. The optimum paths are those that have the lowest maximum altitude along the path. Many such paths exist. The point in common for these paths is the saddle point in some mountain pass whose altitude, if you like, corresponds to the threshold excitation energy a mountaineer must have to cross the mountain.

We have located the saddle points in the potential-energy surface for values of the parameter x between 0.3 and 1.0. The shapes of the liquid drops at typical saddle points are shown in Fig. 46.

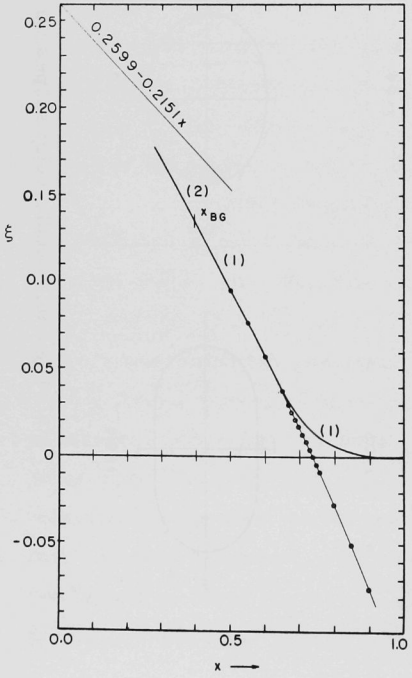

Fig. 47. The relative distortion energy ξ for saddle-point shapes, as a function of x. The numbers in parentheses indicate the degree of instability. Threshold energies correspond to the label (1). The transition from an almost linear dependence on x to an almost cubic dependence on (1 - x) occurs close to x = 0.67. The small circles connected by a thin line correspond to the energy of two equal spheroids whose tips are held at a constant separation. The limiting behavior of ξ at small values of x is indicated in the upper left-hand corner. The significance of x_{BG} is shown in Fig. 49.

In Fig. 47 the energy of these saddle points is given as a function of x. The energy is measured in units of the surface energy of a sphere of unit volume.

In addition to locating the saddle points, we investigated the potential-energy surface in the neighboring region. This was done for both symmetric and asymmetric configurational displacements from the saddle point. The results are most conveniently displayed by given second derivatives of the potential in directions of the usual normal-mode representation. Figure 48 shows the second derivatives c in the lowest two modes for symmetric distortion. The negative value of c_2 indicates that this mode corresponds to the direction of descent away from the saddle point. Its value is an indication of the rapidity of the change in the slope near the saddle point. Similarly the positive values of c_4 indicate that this mode is in the direction of increasing energy.

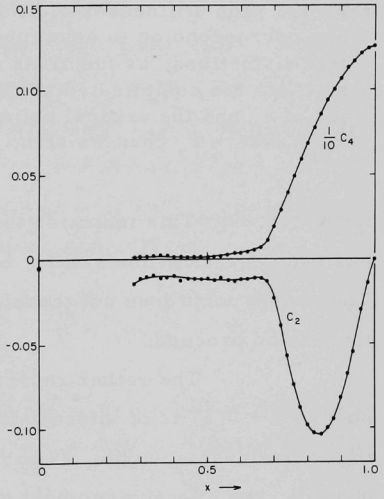

Fig. 48. The stiffnesses c_2 and c_4, corresponding to symmetric distortions, as functions of x. (Note that c_4 is plotted on a scale reduced by 10.) The slight scatter of the points reflects inaccuracies in the numerical procedures which are beginning to show up in the second derivatives c_n.

Figure 49 is a similar plot for the lowest two asymmetric distortions. In particular, c_1 corresponds to a center-of-mass movement (an asymmetric displacement about the plane of symmetry) and should have a true value of 0.0. The errors of our approximate results are therefore indicated in part by this discrepancy. Note that c_3 is negative

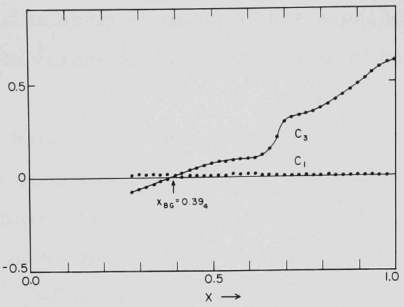

Fig. 49. The stiffnesses c_1 and c_3, corresponding to asymmetric distortions, as functions of x. Note the complicated behavior of c_3 and the critical point x_{BG}, where c_3 changes sign.

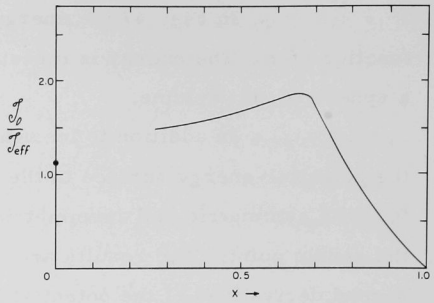

Fig. 50. The reciprocal of the effective moment of inertia $\mathcal{J}_{eff}$, as function of x.

for $x < 0.39$. This indicates that the saddle-point shape for this region has two degrees of instability, one symmetric and one asymmetric. The saddle point does not therefore correspond to a threshold energy for the fission process.

The rather rapid transition of properties in the neighborhood of $x = 0.67$ is of interest since this in fact is the region corresponding to fissionable nuclei. In particular, an experimentally measurable quantity, the effective moment of inertia of the saddle-point shape (Fig. 50) is shown to be rather sensitive to the particular value of x chosen. This indicates that extrapolations in the region around $x = 0.67$ must be done with care.

V-11-1. Resonance Theory of Nuclear Reactions Without Boundary Conditions (51210-01)

Alvin M. Saperstein

The usual attempts to derive a resonance theory for reactions of the type b + B → c + C usually require the separation of space into an inner and outer region, the solution of the Schrödinger equation in the inner region with unphysical boundary conditions, and the matching of the external solutions to the "quasi-bound-state" inner solutions at some fixed channel radius.[1] I have tried to avoid this approach by using the LSZ formalism to derive a Low-type equation from which the resonances may be obtained without any explicit use of a Schrödinger equation, boundary conditions, or separations of the configuration space.

If spin, isotopic spin, and Coulomb effects are neglected, the Lth component of the transition matrix can be written

$$T_{fi}(E, L) = S_{fi}(E, L) + \frac{1}{\pi} \int_0^\infty \frac{\rho_{fi}(E', L)\, dE'}{E' - E - i\epsilon} ,$$

where T_{fi} is the boundary value of a real analytic function in the complex E plane cut along the positive real axis, S is a smooth "source function" (a generalized Born term), and

$$\rho_{fi}(E, L) \equiv \text{Im } T_{fi}(E, L) = \sum_n \bar{p}_n(E, L)\, T^*_{fn}(E, L)\, T_{ni}(E, L) .$$

Here $\bar{p}_n(E, L) \propto \sqrt{E - E_n}$ for $E \geq E_n$ and is zero otherwise; and E_n represents the threshold energies for the allowed intermediate states. We write

---

[1] See, for example, J. Humblet and L. Rosenfeld, Nuclear Phys. 26, 529 (1961), and references therein.

$$\rho_{\alpha\beta} = \sum_{n=1}^{\infty} \left[\theta(E - E_n) - \theta(E - E_{n+1}) \right] \rho_{\alpha\beta}^{\,n},$$

where $\rho_{\alpha\beta}^{\,n}$ can now be defined by analytic continuation for all E. The analytic continuation is obtained by noting that

$$\rho_{\alpha i}^{\,n}(E+i\epsilon) = \sum_{\beta=1}^{n} p_\beta(E+i\epsilon)\, T_{\alpha\beta}(E+i\epsilon) \left[T_{\beta i}(E+i\epsilon) - 2\pi \rho_{\beta i}^{\,n}(E+i\epsilon) \right]$$

so that, by Kramer's rule, $\rho_{\beta i}^{\,n}(E) \equiv \Delta_{\beta i}^{\,n}(E)/\Delta_i^{\,n}(E)$, where

$$\Delta_i^{\,n}(E) = \left| \delta_{\alpha\beta} + 2\pi p_\beta(E)\, T_{\alpha\beta}(E) \right|.$$

Defining $p_\beta(E) \propto \sqrt{E^2 - E_\beta}$ to have a cut along the real E axis from $-E_\beta$ to $+E_\beta$, we see that $\rho^n(E)$ is now a real, meromorphic function in the E plane cut from $-E_n$ to $+E_n$ and from $+E_{n+1}$ to $+\infty$. The poles of $\rho_{\beta i}^{\,n}$ come at the zeroes of $\Delta_i^{\,n}(E)$ which are placed symmetrically with respect to the real E axis. We see that $\rho_{\alpha\beta}$ is a continuous function of E along the real axis but $d\rho/dE$ may not exist at E_n because of the $p_n(E)$ appearing in $\Delta(E)$. This gives rise to the well-known cusps in the scattering amplitude at the threshold energies for new reaction channels. In the neighborhood of a single low-energy isolated pole of $\Delta^n(E)$ at $E = \epsilon_m \pm i\Gamma_m$, we obtain the Breit-Wigner type resonance formula

$$\rho_{\alpha\beta}^{\,n}(E) \approx -\left[\frac{p_0^{\,2}}{p_\alpha p_\beta} \right]^{1/4} \left[\frac{\epsilon_m}{\Gamma_m} \sin(\chi_{\beta 0} + \chi_{\alpha 0}) - \cos(\chi_{\beta 0} + \chi_{\alpha 0}) \right]$$

$$\times \frac{\Gamma_{\alpha m}^{\,1/2}\, \Gamma_{\beta m}^{\,1/2}}{(E - \epsilon_m)^2 + \Gamma_m^{\,2}},$$

where

$$\Gamma_m = \sum_a \Gamma_{am} ,$$

$$\Gamma_{\beta m} \equiv [4 p_\beta p_0]^{1/2} \sin \phi_m \, t_{\beta 0}^2 / q_m ,$$

$$T_{\beta 0}(\epsilon_m) \equiv t_{\beta 0} \, e^{i \chi_{\beta 0}} ,$$

$$q_m \, e^{i \phi_m} \equiv Q_m \equiv 2 \pi \frac{d}{dE} [p_0(E) \, T_{00}(E)]_{E = \epsilon_m} .$$

At present, this work is being continued in the hope of clarifying the relation between the above generalized resonance theory and the formulation of direct interactions as found in a recent preprint.[2]

---

[2] A. M. Saperstein, Calculation of Deuteron Stripping Amplitudes Using S-Matrix Reduction Techniques (to be published).

V-33-5. The Supercurrent State (formerly "Flux Quantization and Time-Reversal Degeneracy") (51300-01)

Murray Peshkin

The method of Byers and Yang[1] has been modified for application to a current-carrying superconducting ring. Discussion is limited to a cylindrical superconducting shell which is thin by the criterion

$$\Delta \Phi << \pi \hbar c / e, \qquad (1)$$

---

[1] N. Byers and C. N. Yang, Phys. Rev. Letters 7, 46 (1961).

where $\Delta\Phi$ is the (external or induced) magnetic flux which passes through the body of the superconductor. This criterion is satisfied in the flux quantization experiments, even though the samples are thick enough to exhibit the Meissner effect. The new feature of this treatment is that in it the zero-order approximate Hamiltonian includes the mutual magnetic interaction of the electron currents. This interaction is then treated by the self-consistent-field method.

It is found that systematic pair degeneracy of single-particle states occurs at values of the induced flux Φ_s which are related to the external flux Φ_e by

$$\Phi_e + (1 + \gamma)\,\Phi_s = n(\pi\hbar c/e), \tag{2}$$

where n is an arbitrary integer. The positive constant γ is given by

$$\gamma = mc^2/\sigma e^2\ , \tag{3}$$

where σ is the number of electrons per unit length of cylinder.

The degenerate pairs at selected values of Φ_s form the basis of a current-carrying BCS state, identical in form to the usual zero-current BCS state, but built on a shifted Fermi sea. The energy of the current-carrying state is equal to that of the zero-current state, except for the kinetic and magnetic energies of the supercurrent.

The presence or absence of the Meissner effect (represented here by the limit $\gamma \to 0$) plays no role in these considerations.

V-38-1. Particles with Zero Mass and Particles with "Small" Mass (51151-01)

F. Coester

The classification of the irreducible representations of the inhomogeneous Lorentz group and explicit realizations of physical interest are well known.[1-7] Representations for zero-mass and nonzero-mass particles are characterized by different invariants and are qualitatively distinct.

On physical grounds one should expect that particles with energies large compared to their mass would be indistinguishable from zero-mass particles. In other words, one should be able to obtain the realizations of the zero-mass representations by continuous transition from the case of nonzero mass. The purpose of this paper is to exhibit this transition explicitly.

The formal limit $m \to 0$ in the usual realization, Eqs. (3) below, leads to a reducible representation. By a simple canonical transformation this realization is automatically reduced in the limit of vanishing mass.

The generators of the inhomogeneous Lorentz group are the space translations $\underset{\sim}{P}$, the time displacement H, the space rotations $\underset{\sim}{J}$, and the proper Lorentz transformation $\underset{\sim}{K}$.

---

[1] E. P. Wigner, Ann. Math. 40, 149 (1939).

[2] V. Bargmann and E. P. Wigner, Proc. Natl. Acad. Sci. U. S. 34, 211 (1948).

[3] B. Bakamjian and L. H. Thomas, Phys. Rev. 92, 1300 (1953).

[4] L. L. Foldy, Phys. Rev. 102, 568 (1956).

[5] Iu. M. Shirokov, J. Exptl. Theoret. Phys. (U.S.S.R.) 33, 861, 1196, 1208 (1957); 34, 717 (1957); 36, 879 (1959).

[6] M. A. Melvin, Revs. Modern Phys. 32, 477 (1960).

[7] J. S. Lomont and H. E. Moses, J. Math. Phys. 3, 405 (1962).

The states of a particle with mass m and spin s may be represented by the function $\psi(\underset{\sim}{p}, \mu)$ with the norm

$$\|\psi\|^2 = \sum_{\mu} \int d\underset{\sim}{p} \, |\psi(\underset{\sim}{p}, \mu)|^2 , \tag{1}$$

where $\underset{\sim}{p}$ is the momentum and μ is the 3 component of the spin $(-s \leq \mu \leq s)$. A complete set of operators operating on these functions is given by $\underset{\sim}{p}$, $\underset{\sim}{x}$, and $\underset{\sim}{s}$, where $\underset{\sim}{x}$ is defined by

$$x_k = i \frac{\partial}{\partial p_k} \qquad (k = 1, \cdots, 3). \tag{2}$$

The spin $\underset{\sim}{s}$ commutes with both $\underset{\sim}{x}$ and $\underset{\sim}{p}$. The three components of $\underset{\sim}{s}$ satisfy the usual commutation rules of angular momenta.

The generators of the Lorentz group are then realized as

$$\begin{aligned} \underset{\sim}{P} &= \underset{\sim}{p} , \\ H &= (p^2 + m^2)^{1/2} \equiv \omega , \\ \underset{\sim}{J} &= \underset{\sim}{x} \times \underset{\sim}{p} + \underset{\sim}{s} , \\ \underset{\sim}{K} &= \tfrac{1}{2}(\underset{\sim}{x}\omega + \omega \underset{\sim}{x}) - \frac{(\underset{\sim}{s} \times \underset{\sim}{p})}{p^2} (\omega - m) , \end{aligned} \tag{3}$$

where $p = |\underset{\sim}{p}|$. It is easy to verify that $(\underset{\sim}{s} \cdot \underset{\sim}{p})/p$ commutes with all generators of the group if $m = 0$. The resulting representation is now reducible except for $s = 0$. If space reflections are included, the representation for $s = \frac{1}{2}$ is still irreducible. Since $\underset{\sim}{x}$ and $\underset{\sim}{s}$ do not commute with $(\underset{\sim}{s} \cdot \underset{\sim}{p})/p$, a complete set of operators on the invariant subspaces is not immediately apparent. It is apparent, however, how we may obtain an equivalent representation that is already reduced in the limit of vanishing mass: We must diagonalize $(\underset{\sim}{s} \cdot \underset{\sim}{p})/p$.

Let U be a unitary operator which commutes with $\underset{\sim}{P}$ and transforms $\underset{\sim}{s}\cdot\underset{\sim}{p}$ according to

$$U^{+}(\underset{\sim}{s}\cdot\underset{\sim}{p})U = ps_{3} \ , \tag{4}$$

and define

$$\begin{aligned} \underset{\sim}{q} &= U\underset{\sim}{x}U^{+} \ , \\ \underset{\sim}{s}' &= U\underset{\sim}{s}U^{+} \ . \end{aligned} \tag{5}$$

If we represent states by functions of $\underset{\sim}{p}$ and the eigenvalue of s_3', then q_k is represented by $i\partial/\partial p_k$. Written as a function of $\underset{\sim}{q}$, $\underset{\sim}{p}$, and s', the generator $\underset{\sim}{J}$ is identical with that given by Shirokov[5] for zero-mass particles. The generator $\underset{\sim}{K}$ becomes identical to Shirokov's zero-mass realization for m = 0. As a possible position operator, $\underset{\sim}{q}$ has the objectionable feature that its commutation relations with $\underset{\sim}{J}$ are not those of a vector.

The following conclusions can be drawn from our results:

(1) Particles with "small" mass behave like particles with zero mass.

The mass m is "small" in this sense if it is small compared to all values of p for which the state function is appreciable.

(2) High-energy particles ($p \gg m$) with definite helicity $(\underset{\sim}{s}\cdot\underset{\sim}{p})/p$ and different spins behave alike.

There still is, of course, the well-known "metaphysical" difference between particles of zero mass and particles of small mass. For zero-mass particles of helicity $\chi \geq 1$, the occurrence of otherwise identical particles with smaller helicity would be an accident. For particles of small mass one must expect such particles unless the interactions conspire not to

produce them. For photons with small mass, this feature has been investigated extensively.[8-11]

A full report has been accepted for publication in the March 15 issue of the Physical Review.

---

[8] L. de Broglie, Mecanique Ondulatoire du Photon et Theorie Quantique des Champs (Gauthier-Villars, Paris, 1949), Chap. 5.

[9] F. J. Belinfante, Progr. Theoret. Phys. (Kyoto) 4, 2 (1949).

[10] F. Coester, Phys. Rev. 83, 798 (1951).

[11] M. M. Bass and E. Schrödinger, Proc. Roy. Soc. (London) 232, 1 (1955).

V-44-1. Foundations of Quantum Mechanics (51300-01)

H. Ekstein

1. A HISTORIC SKETCH

Quantum mechanics is primarily of German origin. Therefore it has an ideological pedigree. It was heralded as the fulfillment of a philosophical program. Heisenberg's "Konzert der Observablen" was a positivistic battle cry, despite its esthetic overtones.

Not much remained of these noble hopes after the dust of the initial skirmishes had settled. Far from dealing with quantities more directly observable than the Bohr-Sommerfeld orbits, quantum mechanics had to state its basic assumptions in terms of nonobservable (complex) wave functions or matrices. The physical interpretation, to be sure, related these unobservable quantities to observables; but it remains an unprecedented departure from the pattern of past physical theories that the subjects of the prime principles of quantum mechanics are not observables.

It was inevitable that some conservatives should try to return to the tradition, and Pascual Jordan made just such an attempt with his "Anschauliche Quantenmechanik." In this theory, the only basic quantities are observables, and the principles are couched in operational terms. The hope was that such a formulation could be shown, by purely deductive manipulations, to be equivalent to either conventional quantum mechanics or—and this is where the excitement of discovery begins—to some other, more general theory.

Jordan assumed that the following operations between observables are operationally defined: addition, multiplication by real numbers, and squaring. The algebra of observables so defined—the Jordan algebra—can be realized or represented by operators on Hilbert space, and thus one can recover conventional quantum mechanics. But is this realization unique? If not, we have not really gained much; by choosing a particular representation, we have again smuggled nonphysical, unobservable assumptions into our principles.

Later studies of this question by a number of investigators—including Wigner, v. Neumann, and Segal—showed that in order to obtain some reasonably restricted choice of theories, a number of "topological" axioms had to be adjoined to Jordan's original set, i.e., statements concerning the limits of sequences of observables. Such axioms are, by their nature, not readily verified by experiment, and this seems to be a serious defect of the entire approach.

Another objection concerns the basic assumptions of Jordan. Is it legitimate to assume that observables can be added and squared? For instance, if p and q are "noncommuting" observables, is it possible to design a procedure (p + q) which will have the same frequency distribution of measurements as the sum of the distributions of p and of q? Nobody has been bold enough to offer such prescriptions, and therefore the genuinely operational (probably the best translation for "anschaulich"—not philologically, but operationally) nature of Jordan's theory is in doubt.

These considerations may have motivated v. Neumann and G. Birkhoff to explore a radically different avenue to the foundations of quantum mechanics. They investigated the "logic," i.e., the calculus of propositions, in physical theories of a nonclassical type. Unfortunately, it is not easy to relate a postulated logical relations to experiment, so that the verification seems to be again very indirect. What is more, quantum mechanics does not fit into the scheme (modular lattices) which v. Neumann and Birkhoff consider as plausible. Perhaps as a consequence of these difficulties, the entire field has been deserted by physicists and taken over by philosophers of the more mathematically inclined type, expecially French. This author is unable to evaluate their contributions.

2. A NEW APPROACH

It may be a sign of decline that physicists are again becoming interested in questions of foundations; perhaps there is a lack of exciting news of pragmatic nature. However that may be, there is a revival of interest, and this author has an idea to contribute.

Classical mechanics deals almost entirely with pure, i.e., completely determined processes. Statistical mixtures are usually considered almost as an afterthought. In other words, it is found convenient to deal with "delta functions" rather than more general measures on phase space.

Translation of this remark to quantum mechanics puts emphasis on pure states, as contrasted to statistical mixtures, i.e., on one-dimensional projections. Instead of trying to formulate axioms with respect to general ensembles, we concentrate on pure states.

The essentially new assumption is that to every pure state f there is associated an observable (a question) Q_f, which has only Yes (1) or No (0) in its range, and which has expectation value 1 with respect to the pure state f, and less than 1 with respect to any other state g, i.e.,

$$\underset{\underset{\sim}{g}}{\mathrm{Exp}}\ \underset{\sim}{Q}_{\underset{\sim}{f}} \begin{cases} = 1 & \underset{\sim}{f} = \underset{\sim}{g}\,, \\ < 1 & \underset{\sim}{f} \neq \underset{\sim}{g}\,. \end{cases} \tag{1}$$

Let us consider the nature of $\underset{\sim}{Q}_{\underset{\sim}{f}}$ for classical physics. This $\underset{\sim}{Q}_{\underset{\sim}{f}}$ is, quite literally, the question: are you $\underset{\sim}{f}$? And in classical physics, a pure state is either never or always found to be $\underset{\sim}{f}$. Hence $\underset{\underset{\sim}{g}}{\mathrm{Exp}}\ \underset{\sim}{Q}_{\underset{\sim}{f}} = 0$ if $\underset{\sim}{f} \neq g$. This is a special case of our Eq. (1).

It is postulated furthermore that the expectation value of the question: "are you $\underset{\sim}{f}$?" with respect to the pure state $\underset{\sim}{g}$ is the same as the expectation value of the question: "are you $\underset{\sim}{g}$?" with respect to the state $\underset{\sim}{f}$, i.e.,

$$\underset{\underset{\sim}{f}}{\mathrm{Exp}}\ \underset{\sim}{Q}_{\underset{\sim}{g}} = \underset{\underset{\sim}{g}}{\mathrm{Exp}}\ \underset{\sim}{Q}_{\underset{\sim}{f}}\,.$$

Statements concerning pure states can be verified by detailed consideration of experiments such as polarization. They are always operational. It is true that these experiments are always dealing, in effect, with only a finite number of "degrees of freedom."

With a reasonably small number of such postulates, it seems possible to build a scheme which is mathematically equivalent to quantum mechanics.

During a recent conversation with R. Haag, it was discovered that he and Araki have had a very similar idea and are working on it. We may combine our efforts in this investigation.

PUBLICATIONS SINCE THE LAST REPORT

PAPERS

MASS SPECTROMETRIC STUDY OF THE MAGNESIUM HALIDES
J. Berkowitz and J. R. Marquart . . . . . .(Project II-29)
J. Chem. Phys. 37, 1853-1865 (October 15, 1962)

ON THE IONIZATION POTENTIAL OF THE CH_2 RADICAL
J. Berkowitz and S. Wexler . . . . . .(Project II-29)
J. Chem. Phys. 37, 1476-1478 (October 1, 1962)

NEUTRON DETECTION WITH GLASS SCINTILLATORS
L. M. Bollinger, G. E. Thomas, and R. J. Ginther . .(Project I-2)
Nuclear Instr. and Methods 17, 97-116 (1962)

SCATTERING OF ALPHA PARTICLES BY Zn^{64} AND Zn^{68}
H. W. Broek, T. H. Braid, J. L. Yntema, and
B. Zeidman . . . . . .(Project I-22)
Nuclear Phys. 38, 305-315 (1962)

STATES IN B^{10} FROM ELASTIC SCATTERING OF ALPHAS BY Li^6
G. Dearnaley, D. S. Gemmell, and S. S. Hanna. .(Unattached)
Nuclear Phys. 36,71-81 (July 1962)

NEUTRON BACKGROUND DUE TO Ta BACKINGS FOR LITHIUM TARGETS
C. T. Hibdon . . . . . .(Project I-98)
Nuclear Instr. and Methods 17, 177-180 (1962)

"
THE MOSSBAUER EFFECT IN METALLIC IRON
R. S. Preston, S. S. Hanna, and J. Heberle . . .(Project I-19)
Phys. Rev. 128, 2207-2218 (December 1, 1962)

RADIATION SHIELDING STUDIES AT THE NAVAL CIVIL ENGINEERING LABORATORY
H. E. Stanton . . . . . (Unattached)
Naval Research Reviews (November 1962), pp. 13-16

A BORON-LOADED LIQUID SCINTILLATION NEUTRON DETECTOR USING A SINGLE PHOTOMULTIPLIER
G. E. Thomas . . . . . .(Project I-22)
Nuclear Instr. and Methods 17, 137-139 (1962)

ABSTRACTS

New York meeting of the American Physical Society, January 23-26, 1963.

$K^{39}(p,\alpha)Ar^{36}$ REACTION
R. G. Allas, D. von Ehrenstein, L. Meyer-Schützmeister, and J. A. Weinman . . . . . (Project I-21)
Bull. Am. Phys. Soc. 8, 48 (23 January 1963)

REACTION $B^{11}(p,\gamma)C^{12}$ IN THE RANGE $4 < E_p < 10$ MEV
R. G. Allas, S. S. Hanna, L. L. Lee, Jr., L. Meyer-Schützmeister, and R. E. Segel . . . . . (Project I-21)
Bull. Am. Phys. Soc. 8, 11 (23 January 1963)

A STUDY OF THE $Ca^{40}(d,d)Ca^{40}$ AND $Ca^{40}(d,p)Ca^{41}$ REACTIONS
L. L. Lee, Jr., J. P. Schiffer, and B. Zeidman. .(Project I-27)
Bull. Am. Phys. Soc. 8, 48 (23 January 1963)

REGGE TRAJECTORY IN FIELD THEORY
L. S. Liu and K. Tanaka . . . . . (Project V-45)
Bull. Am. Phys. Soc. 8, 44 (23 January 1963)

ACM STUDENT REPORTS

MASS SPECTROMETRIC STUDIES OF THE DIFFUSION OF ALKALI SALTS THROUGH PLATINUM
E. S. Bliss . . . . . (Project II-24)
ACM student report to Lawrence College (January 1963)

THE MÖSSBAUER CROSS SECTION IN IRON-57 AT ROOM TEMPERATURE
W. Denno . . . . . .(Project I-19)
ACM student report to Kalamazoo College (February 1963)

MEASUREMENT OF THE GAMMA DECAY OF W^{188}
W. E. Gelhaar . . . . . (Project I-36)
ACM student report to Knox College (January 1963)

ADDITIONAL PAPERS ACCEPTED FOR PUBLICATION

PARTICLES WITH ZERO MASS AND PARTICLES WITH "SMALL" MASS
F. Coester . . . . . (Project V-38)
Phys. Rev. (March 15, 1963)

THREE-NEUTRINO HYPOTHESIS
K. Hiida . . . . . (Project V-47)
Nuovo cimento

Σ BREAKUP AND THE $\Sigma\Lambda$ RELATIVE PARITY
K. Hiida, J. L. Uretsky, and R. J. Oakes . . . (Project V-47)
Nuovo cimento

A TEST OF THE STATISTICAL NATURE OF FLUCTUATIONS IN NUCLEAR CROSS SECTIONS
L. L Lee, Jr. and J. P. Schiffer . . . . . (Project I-31)
Phys. Letters 4 (1 March 1963)

STEREOSCOPIC TELEVISION SYSTEM
W. J. O'Neill . . . . . (Project I-22)
Nuclear Instr. and Methods

POSSIBLE DETERMINATION OF THE SPIN OF Ξ^- FROM ITS DECAY ANGULAR ASYMMETRY
M. Peshkin . . . . . (Project V-5)
Phys. Rev. (February 15, 1963)

(n,2n) REACTION CROSS SECTIONS FROM 12 to 19.6 MEV
L. A. Rayburn . . . . . (Project I-90)
Phys. Rev.

THE GAMMA-RAY SPECTRUM FROM THERMAL NEUTRON CAPTURE IN Hf^{177} AND ASSOCIATED ENERGY LEVELS IN Hf^{178}
R. K. Smither . . . . . (Project I-60)
Phys. Rev. (February 1, 1963)

A NOTE ON THE MEASURABLE ELECTRIC CHARGE OF SPIN-$\frac{1}{2}$ BOSONS
R. Spitzer . . . . . (Project V-39)
Nuovo cimento

ON THE MECHANISM OF THE ISOTOPIC EXCHANGE OF TRITIUM WITH METHANE

S. Wexler . . . . . .(Project II-41)

J. Am. Chem. Soc. (February 1963)

PERSONNEL CHANGES IN THE ANL PHYSICS DIVISION

NEW MEMBERS OF THE DIVISION

Student Aide (Co-op)

Mr. Gordon Hoffman, Illinois Institute of Technology. Working with L. S. Goodman on a field stabilizer for atomic-beam magnetic-resonance machines. Came to ANL on January 28, 1963.

Student Aides (ACM)

Mr. David J. Bailey, Beloit College. Working with S. S. Hanna on measurements of intensities and isomer shifts in the Mössbauer effect in Fe^{57}. Came to ANL on February 4, 1963.

Mr. Joel Terrence Klopcic, Knox College. Working with M. S. Kaminsky on ionic impact phenomena on metal surfaces. Came to ANL on January 28, 1963.

Mr. Michael Peter Schulhof, Grinnell College. Working with J. Heberle on the application of a superconducting magnet to Mössbauer experiments. Came to ANL on January 28, 1963.

Mr. Leighton R. Scott, Knox College. Working with S. B. Burson on the β and γ spectroscopy of several isotopes,

especially W^{188} and Re^{188}. The study will include angular-correlation measurements and the use of computer programs for analysis of β and γ spectra. Came to ANL on January 28, 1963.

PROMOTIONS

Dr. Morton Hamermesh, who has been Director of the ANL Physics Division since April 1, 1959, was appointed Associate Director of the Laboratory on February 15, 1963. In this capacity he will help coordinate basic scientific research in all divisions of the Laboratory.

Dr. Lowell M. Bollinger was made Director of the ANL Physics Division on February 20, 1963.

Dr. Murray Peshkin was made Associate Director of the ANL Physics Division on February 2, 1963. He will be concerned with administrative matters in the theoretical section and with general policy for the division as a whole.